Research Paper

Novel necroptosis-related gene signature for predicting the prognosis of pancreatic adenocarcinoma

Zixuan Wu[1], Xuyan Huang[1], Minjie Cai[2], Peidong Huang[3], Zunhui Guan[4]

[1]Guangzhou University of Chinese Medicine, Guangzhou, Guangdong Province 510006, China
[2]Shantou Health School, Shantou, Guangdong Province 515061, China
[3]Yunnan University of Chinese Medicine, Kunming, Yunnan Province 650500, China
[4]Kunming Municipal Hospital of Traditional Chinese Medicine, Kunming, Yunnan Province 650011, China

Correspondence to: Peidong Huang; **email:** huangpeidong@ynutcm.edu.cn
Keywords: pancreatic adenocarcinoma (PAAD), necroptosis-related genes (NRGs), TCGA and GEO datasets, immunity, m6A and immune checkpoint, bioinformatics analysis
Received: November 4, 2021 **Accepted:** January 11, 2022 **Published:** January 24, 2022

ABSTRACT

Pancreatic adenocarcinoma (PAAD) is a deadly digestive system tumor with a poor prognosis. Recently, necroptosis has been considered as a type of inflammatory programmed cell death. However, the expression of necroptosis-related genes (NRGs) in PAAD and their associations with prognosis remain unclear. NRGs' prediction potential in PAAD samples from The TCGA and GEO datasets was investigated. The prediction model was constructed using Lasso regression. Co-expression analysis showed that gene expression was closely related to necroptosis. NRGs were shown to be somewhat overexpressed in high-risk people even when no other clinical symptoms were present, indicating that they may be utilized in a model to predict PAAD prognosis. GSEA showed immunological and tumor-related pathways in the high-risk group. Based on the findings, immune function and m6A genes differ significantly between the low-risk and high-risk groups. MET, AM25C, MROH9, MYEOV, FAM111B, Y6D, and PPP2R3A might be related to the oncology process for PAAD patients. Moreover, CASKIN2, TLE2, USP20, SPRN, ARSG, MIR106B, and MIR98 might be associated with low-risk patients with PAAD. NRGs and the relationship of the immune function, immune checkpoints, and m6A gene expression with NRGs in PAAD may be considered as potential therapeutic targets that should be further studied.

INTRODUCTION

Pancreatic adenocarcinoma (PAAD) is considered as a fatal gastrointestinal tumor globally, with a death rate that is comparable to its incidence [1]. Surgical resection is the only drastic therapy, but the prognosis is dismal. Primary screening of high-risk factors of PAAD has no standard. By contrast, CT, MRI, positron emission tomography/computed tomography is utilized to diagnose PAAD [2]. However, most patients with PPAD are already in advanced stages, and they have missed the opportunity for surgical treatment after being diagnosed. The curative impact of radiation and chemotherapy for PAAD is not precise [3]. Considering that molecularly targeted therapy has become an indispensable method of treating malignant tumors, identifying novel therapeutic targets is critical.

Apoptosis resistance is a significant barrier that causes chemotherapy to fail during cancer treatment. Bypassing the apoptotic pathway to increase cancer cell death can be performed to address this problem [4, 5]. When apoptosis cannot occur properly, the cell will die. Necrosis is initiated as a "substitute" for apoptosis [6]. It is a caspase-independent, regulated necrotic cell death mechanism primarily mediated by receptor-interacting Protein 1 (RIP1), RIP3, and mixed lineage kinase

domain-like protein (MLKL) [7]. Necrotic cells will expel their contents, stimulating the inflammatory response of the surrounding cells and activating body's immunological response. Consequently, cell necrosis plays a significant role in tumorigenesis, metastasis, and infectious and inflammatory disorders [8, 9]. Necroptosis promotes cancer spread, although it could suppress cancer [10–12]. However, only a few sequence-based studies on aberrant gene expression and its relationship with overall survival (OS) in PAAD patients with necroptosis have been conducted.

Immune checkpoint-related gene profiles in patients with PAAD may be used to identify, evaluate, and

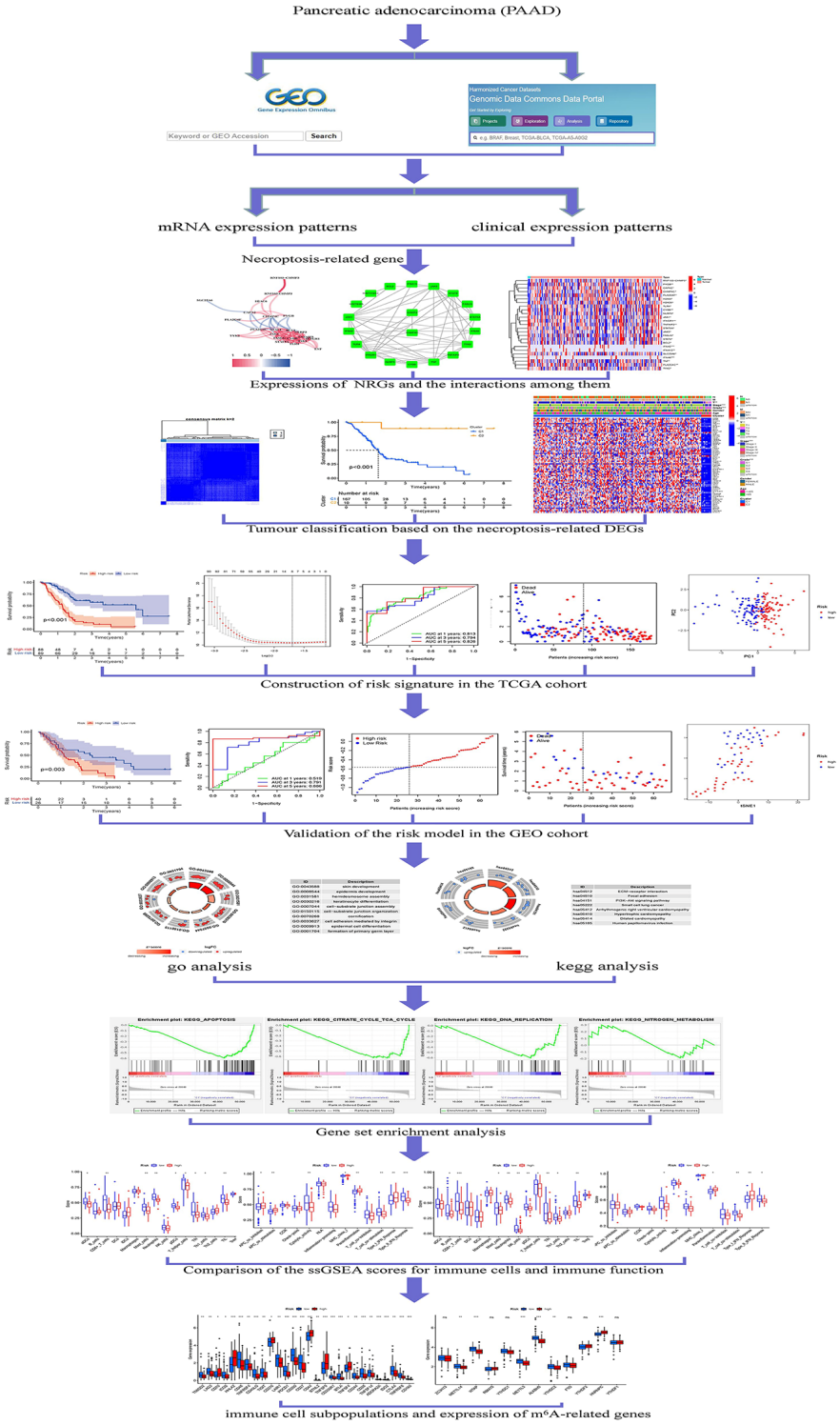

Figure 1. Framework based on an integration strategy of NRGs.

predict treatment responses [13]. Despite little analysis conducted on the link between NRGs and PAAD, studying the interaction between NRGs, immunity, immunological checkpoints, and m6A with PAAD clinicopathological tumor options is important. The cause and mechanism of PAAD's abnormal gene expression and necroptosis are unknown. Further research on the altered transcription of NRGs in patients with PAAD is required to investigate the influence of the NRGs pathway on the prognosis of patients with PAAD. Therefore, understanding the impact of NRGs on PAAD development may find a biomarker that might be utilized as a therapeutic target.

This study aimed to form a prognostic model for PAAD prognosis by spotting NRGs expression related to PAAD patient prognosis. Comprehensively understanding the invasion of NRGs and their associated targets, innovative PAAD therapeutic targets and pharmacologic approaches will be developed. The strategy of NRGs is shown in Figure 1.

MATERIALS AND METHODS

We followed the methods of Ying Ye et al. 2021 [14].

Datasets and NRGs

PAAD gene expression patterns and clinical data were collected from the Cancer Genome Atlas (TCGA) [15]. In September 30, 2021, the data of 181 PAAD and 4 normal tissues were enrolled in the TCGA. The Gene Expression Omnibus (GEO) was searched for micro data on mRNA expression. Series: GSE62452. Platform: GPL6244. The GEO shared database was used to maintain the expression patterns of 130 PAAD cases (Table 1). In addition, 52 NRGs were identified from KEGG (https://www.kegg.jp/kegg/) (Supplementary Table 1).

Annotation of genes, identification of NRGs and its mutation rates

Transcription and human configuration data were matched by Perl to obtain the precise mRNA gene expression data. The gene IDs were transformed into gene names by R4.1.0 [16]. In order to evaluate the difference of NRGs expression (DEGs) with statistical significance, FDR <0.05 and |log2FC|≥0.585 as a selection criteria. DEG mutation rates were examined using Cbioportal [17] (http://www.cbioportal.org/).

Tumor classification based on DEGs

First, prognosis-related NRGs were classified into two groups: cluster 1 and 2. Survminer and survival were used to explore the survival and predictive value of PRG subtypes. pheatmap was used to construct a heatmap showing the differential expression and the relationship between NRGs and clinicopathological features of NRGs in each cluster. Limma and corrplot were used to explore the gene connection between PAAD target genes and prognostic NRGs.

Development of NRGs prognostic signature

The DEGs were split into two classes that supported the median score: low-and high-risk. Lasso regression was related to two classes, and the boldness interval and risk ratio were computed. Survival curves for the two groups were generated and compared. timeROC was used to provide a comparable receiver-operating characteristic (ROC) curve to evaluate the accuracy of this model for predicting survival in PAAD. For the chance curve bestowed by the risk score, NRGs' risk and survival status were examined. The relationship between clinical characteristics and risk-model was determined, and a similar relationship was found between two NRGs patients. Analyses of risk and clinical relationships are distributed. In addition, investigation was performed using principal component analysis (PCA) and T-distributed neighbor embedding (T-SNE) to analyze whether the prognostic model might properly categorize patients into two risk teams [18]. Desegregating the prognosticative signals, a representation was developed to predict 1-, 3-, and 5-year OS of patients with PAAD.

Functional enrichment of differentially expressed NRGs

The biological pathways associated with the TCGA DEGs were then examined using Gene Ontology (GO). Biological processes (BP), molecular functions (MF), and cellular components (CC) are controlled by differentially expressed NRGs. NRGs were further investigated using R based on KEGG data [19].

GSEA enrichment analyses and predictive nomogram

GSEA was used to find related functions and pathway variations. The associated score and graphs were used to verify whether the functions and routes within different risk groups were dynamic. Every sample was classified as "H" or "L" based on whether it had been a high-risk cluster of prognosis-related NRGs.

Comparison of immune activity among subgroups

Analysis of single-sample sequence set enrichment was utilized (ssGSEA). The enrichment score of immune cells and immune-related activities in two groups was examined in each TCGA and GEO cohort. In addition,

Table 1. Clinical characteristics.

TCGA		GEO	
Variables	**Number of samples**	**Variables**	**Number of samples**
Gender		Gender	
Male/Female	102/83	Male/Female	Unknown
Age at diagnosis		Age at diagnosis	
≤65/>65	96/89	≤65/>65	Unknown
Grade		Grade	
G1/G2/G3/G4/NA	32/97/51/2/3	G1/G2/G3/G4/NA	3/64/59/2/2
Stage		Stage	
I/II/III/IV/NA	21/152/4/5/3	I/II/III/IV/NA	7/84/26/13/6
T		T	
T1/T2/T3/T4/NA	7/24/148/4/2	T1/T2/T3/T4	Unknown
M		M	
M0/M1/NA	85/5/95	M0/M1/NA	Unknown
N		N	
N0/N1/N2	80/130/5	N0/N1/N2/N3	Unknown

the connection among NRGs, checkpoints, and m6A were investigated because these NRGs had significant therapeutic implications.

Data availability

Patients who granted informed consent to use their data have been uploaded to the public-accessible TCGA and GEO databases.

Ethics approval and consent to participate

This manuscript is not a clinical trial; hence, ethics approval and consent to participate is not applicable.

RESULTS

Differentially expressed NRGs

We found 25 DEGs related to TCGA (7 upregulated, 18 downregulated; Figure 2A, Supplementary Table 2). We performed a protein–protein interaction (PPI) study to investigate NRGs' interactions, and the findings are presented in Figure 2B. We discovered that JAK1, TNF, JAK3, IFNGR1, TLR4, and TYK2 were hub genes by setting the low necessary interaction value to 0.4. (Supplementary Table 3). These genes, which included all DEGs discovered in normal and malignant tissues, may be used to determine independent PAAD prognostic markers. Figure 2C demonstrates the correlation network, which includes all NRGs. We investigated genetic changes in these NRGs because of their important clinical implications. We found that the two common mutations were truncating and missense mutations (Figure 3). A total of 9 genes had a 3% mutation rate, with IFNA2, IFNA6, and IFNA13 being the commonly altered (17%).

Tumor classification based on the DEGs

According to Consensus clustering analysis, when the clustering variable (k) was set to 2, the intragroup correlations were the highest, and the intergroup correlations were the lowest, indicating that the 181 PAAD patients could be separated into two groups (Figure 4A). Consequently, DEGs were divided into two clusters: cluster 1 and 2. The gene expression profile and clinical features were shown using a heatmap (Figure 4B). Survival research was conducted to evaluate the prognostic value of NRGs, and the survival rate of cluster 2 was higher than that of cluster 1 ($P < 0.001$, Figure 4C).

Development of a prognostic gene model in the TCGA cohort

We incorporate the TCGA cohort in the training group and the GEO Cohort in the test group to improve the accuracy of the prognostic model. The university COX study identified 10 significant NRGs, which were then included in multivariate COX analysis. A total of 10 NRGs were identified as independent PAAD prognostic markers (MET, CASKIN2, TLE2, USP20, MROH9, SPRN, ARSG, ARNTL2, ANLN, LY6D;

Figure 5A). A gene signature was created using the absolute minimal shrinkage and selection operator (LASSO) Cox regression analysis and optimal value (Figure 5B, 5C). We discovered that the risk score of patients was negatively connected to the survival of patients with PAAD. Most of the new NRGs discovered in this investigation showed a negative relationship with the risk model, indicating that additional research is necessary (Figure 5D). Based on Kaplan–Meier analysis, the presence of high-risk PRG signatures was linked with a decreased chance of survival ($P < 0.001$, Figure 5E). For 1, 3, and 5-year survival rates, the AUC predictive value of the unique NRGs signature was 0.813, 0.794, and 0.826, respectively (Figure 5F). The PCA and t-SNE results showed that patients with varying risks were divided into two groups (Figure 5G, 5H).

External validation of the risk signature

A GEO cohort of 130 PAAD patients served as the validation group. We discovered that patient's risk score

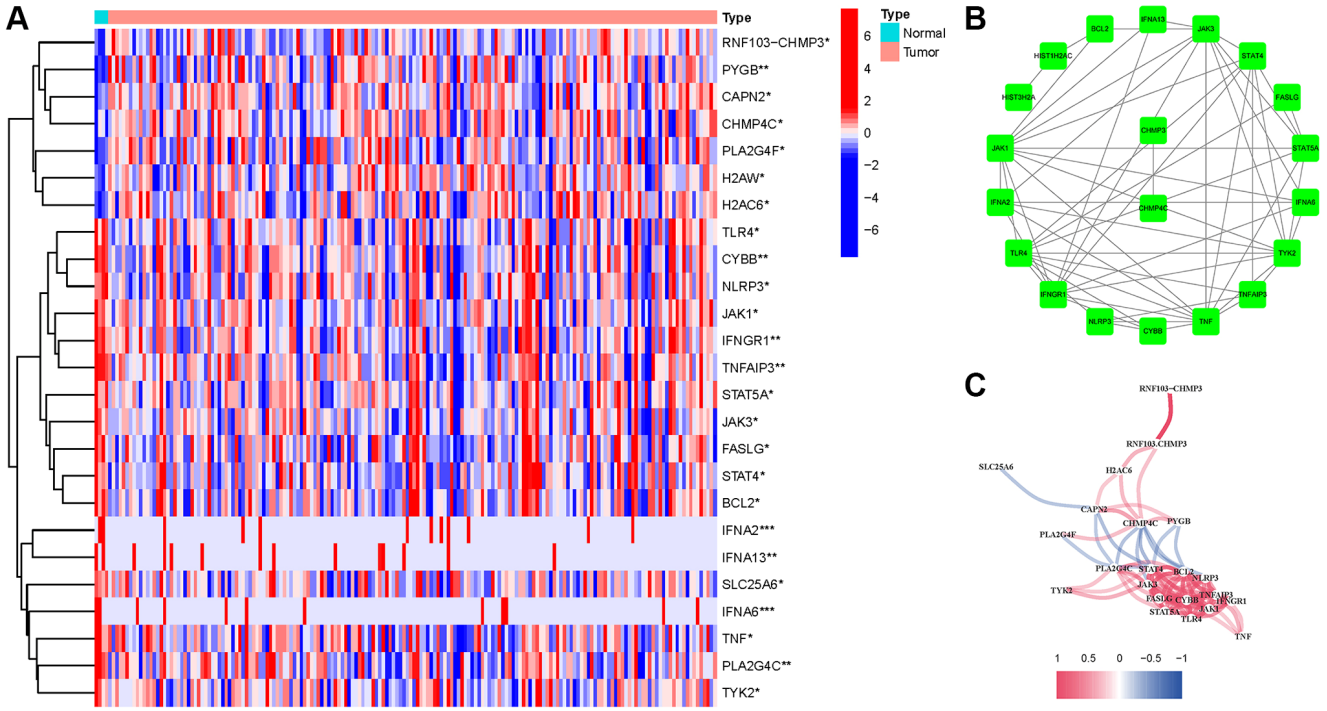

Figure 2. Expressions of the 25 NRGs and their interactions. (**A**) Heatmap. (**B**) PPI network. (**C**) Correlation network (red: positive; blue: negative).

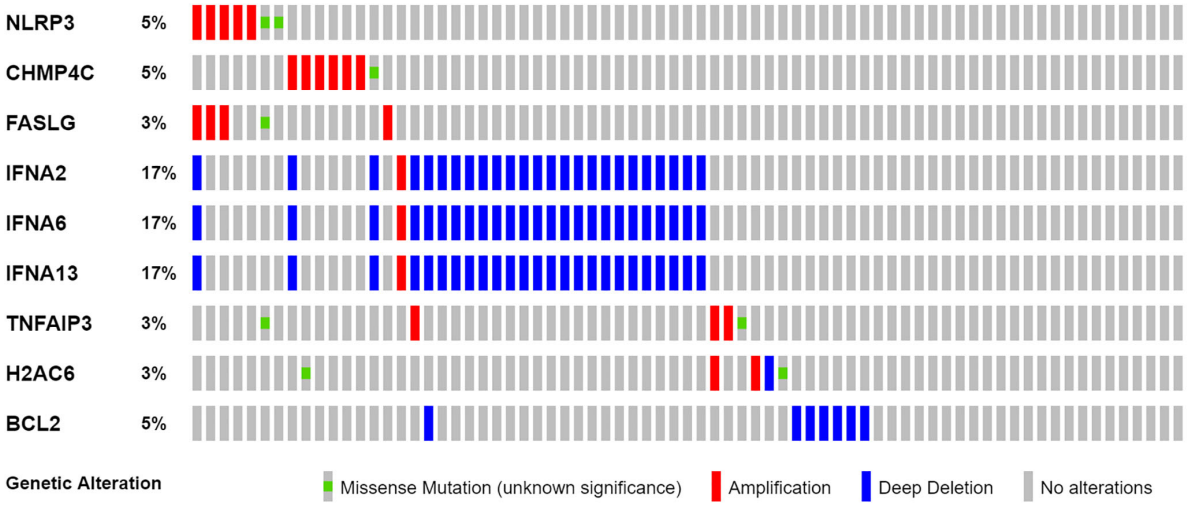

Figure 3. Mutations in NRGs (Abbreviations: N: normal; T: tumor).

was negatively related to the survival of patients with PAAD. Similar to the TCGA findings, most of the novel NRGs discovered in this investigation were adversely linked with the risk model (Figure 6A). The presence of high-risk PRG signatures was associated with a lower likelihood of survival (P = 0.003). Kaplan-Meier analysis was utilized to create Figure 6B. The AUC predictive value of the unique NRGs signature was 0.519, 0.791, and 0.886 for 1, 3, and 5-year survival rates, respectively (Figure 6C). The results of PCA and t-SNE revealed that patients with varied risks were well divided into two groups (Figure 6D, 6E).

Independent prognostic value of the risk model

COX analysis in the TCGA cohort revealed that the NRGs signature (HR: 37.625, 95CI: 15.601-90.741) was the primary independent predictor of OS of patients with PAAD (HR: 37.625, 95CI: 15.601–90.741; Figure 7A, 7B). The COX analysis result was demonstrated in the GEO cohort (Figure 7C, 7D). In addition, we created a heatmap of clinical features for the TCGA cohort (Figure 7E, Supplementary Table 4).

Enrichment analysis of necroptosis-related genes

GO enrichment analysis revealed 83 core targets, including CC and BP. The CC primarily involves the cell–substrate junction (GO:0030055), endoplasmic reticulum lumen (GO:0005788), and basal part of cell (GO:0045178). The BP primarily involves ameboidal-type cell migration (GO:0001667), epidermis development (GO:0008544), epithelial cell proliferation (GO:0050673), and cell junction assembly (GO:0034329, Supplementary Table 5A). In addition, the main signaling pathways were identified by KEGG enrichment analysis, revealing that the over-expressed genes were primarily involved in the PI3K-Akt signaling pathway (hsa04151), focal adhesion (hsa04510), dilated cardiomyopathy (hsa05414), and small cell lung cancer (hsa05222, Figure 8 and Supplementary Table 5B).

Gene set enrichment analyses

Based on gene set enrichment analyses (GSEA), the majority of NRGs prognostic signature regulated immune and tumor-related pathways such as proteasome, steroid biosynthesis, pentose phosphate pathway, aminoacyl tRNA biosynthesis, p53, notch, and wnt signaling pathway. The top 6 enriched functions or pathways for each cluster are shown in Figure 9 and Supplementary Table 6A, 6B. Consequently, the "p53 signaling pathway" was the most enriched.

Comparison of the immune activity among subgroups

We evaluated the enrichment scores of 16 kinds of immune cells and the activity of 13 immune-related functions across low- and high-risk groups (ssGSEA). aDCs, DCs, iDCs, macrophages, Th2 cells, and Treg did not differ substantially between the two groups

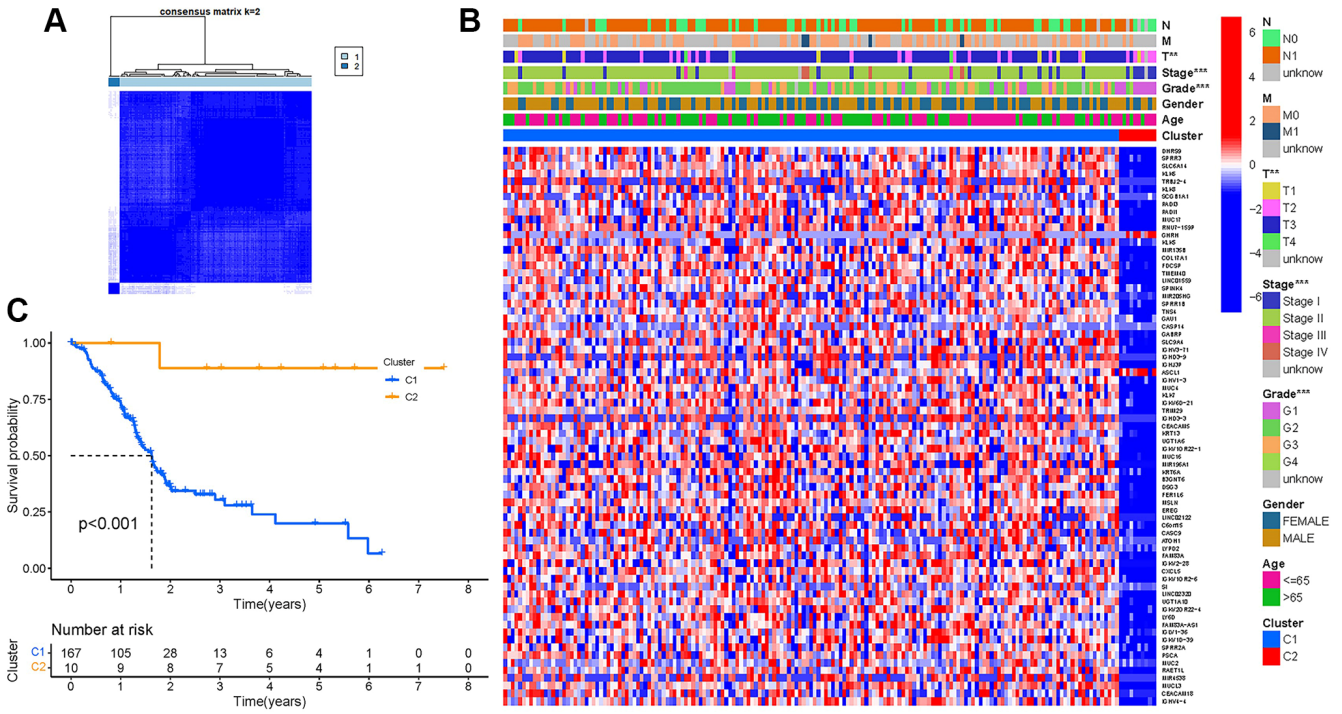

Figure 4. Tumor classification. (**A**) Consensus clustering matrix (k = 2). (**B**) Heatmap. (**C**) Kaplan–Meier OS curves.

in the TCGA cohort ($P > 0.05$). Other immune cells infiltrate at a greater rate in the high-risk subgroup (Figure 10A). CCR, check point, HLA, inflammation-related promotion, and T cell co-inhibition were not substantially different between the two groups ($P > 0.05$). Other immune-related functions are usually more significant in the high-risk group (Figure 10B). Similar findings were reached when examining the immunological state of the GEO cohort (Figure 10C, 10D).

Analysis of the correlation among NRGs with immune checkpoints and m6A

We investigated potential changes in immune checkpoint expression and m6A genes between the two groups. The expression of HHLA2, CD48, CD40LG, PDCD1, CD200, CD27, and other genes differed significantly between the two patient groups (Figure 11A). When the PRG expression was examined between the two-risk groups, METTL3, METTL14, HNRNPC, WTAP, YTHDC2, and ALKBH5 were substantially more significant in the high-risk group (Figure 11B). HNRNPC associated with m6A modification had higher expression in high risk group, suggesting that it might be related to the oncology process for PAAD patients. While METTL14, WTAP, METTL3, ALKBH5, and YTHDC2 had lower expression in high risk group, indicating that they might be tumor suppressor.

DISCUSSION

Treating PAAD is a severe clinical issue because of its advanced stages and terrible illness [20]. The molecular identification of diagnostic biomarkers and treatment

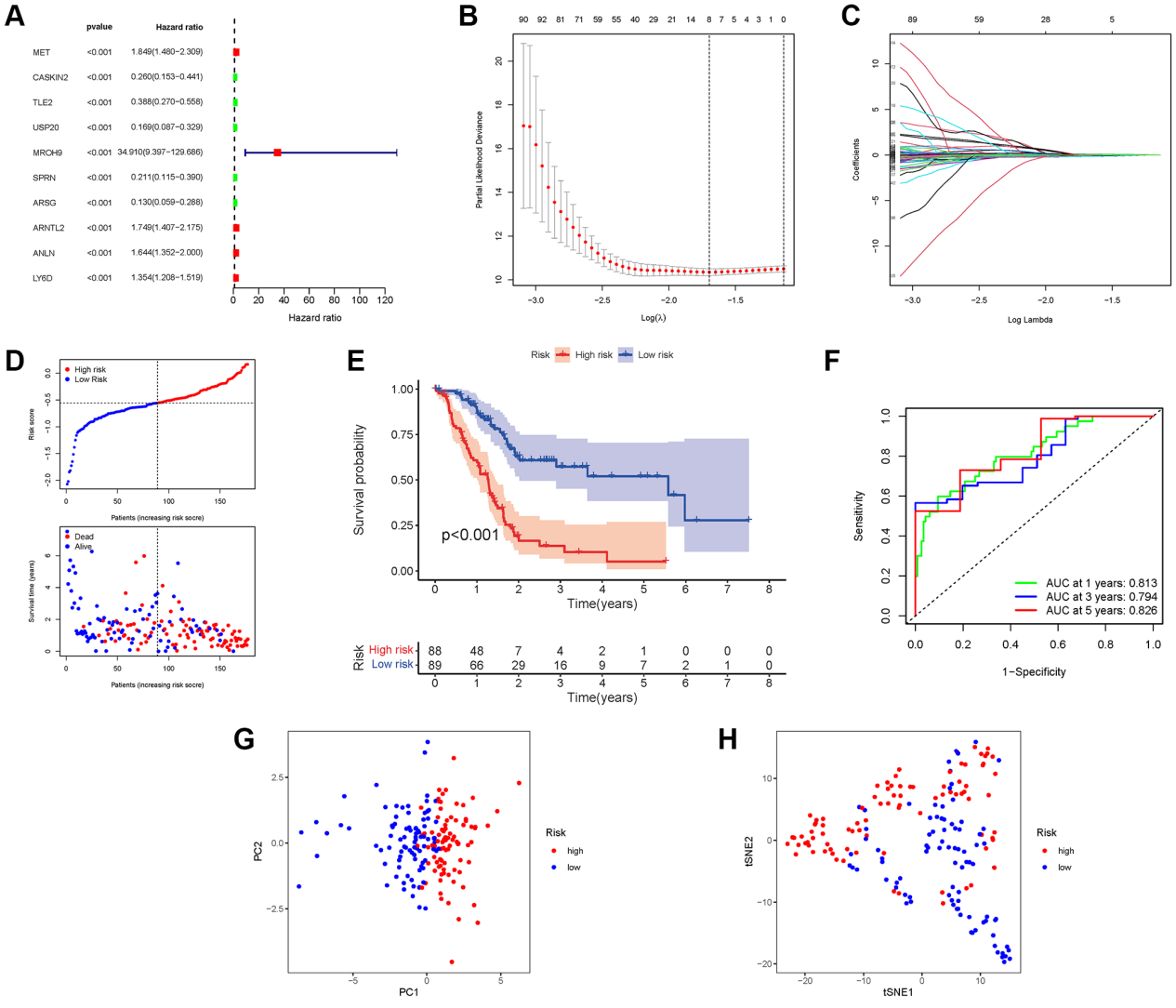

Figure 5. Construction of risk signature in the TCGA cohort. (**A**) Univariate cox regression analysis of OS. (**B**) LASSO regression of OS-related genes. (**C**) Cross-validation for tuning the parameter selection. (**D**) Risk survival status plot. (**E**) Kaplan–Meier curve result. (**F**) The AUC of the prediction of 1, 3, 5-year survival rate of PAAD. (**G**) PCA plot. (**H**) t-SNE plot.

targets for PAAD should always be prioritized. Previous research has shown that vanadium complexes have a selective cytotoxic effect on the human pancreatic ductal adenocarcinoma cell line (PANC-1), causing the mixture of apoptotic and necroptotic processes of PANC-1 cells at increasing doses [21]. Necroptotic programmed cell death is an alternate method of programmed cell death, which can address apoptosis resistance and activate and enhance antitumor immunity in cancer treatment [22]. Necroptosis can serve as a tumor suppressor, making it a potentially practical cancer therapy approach [23]. This research has been

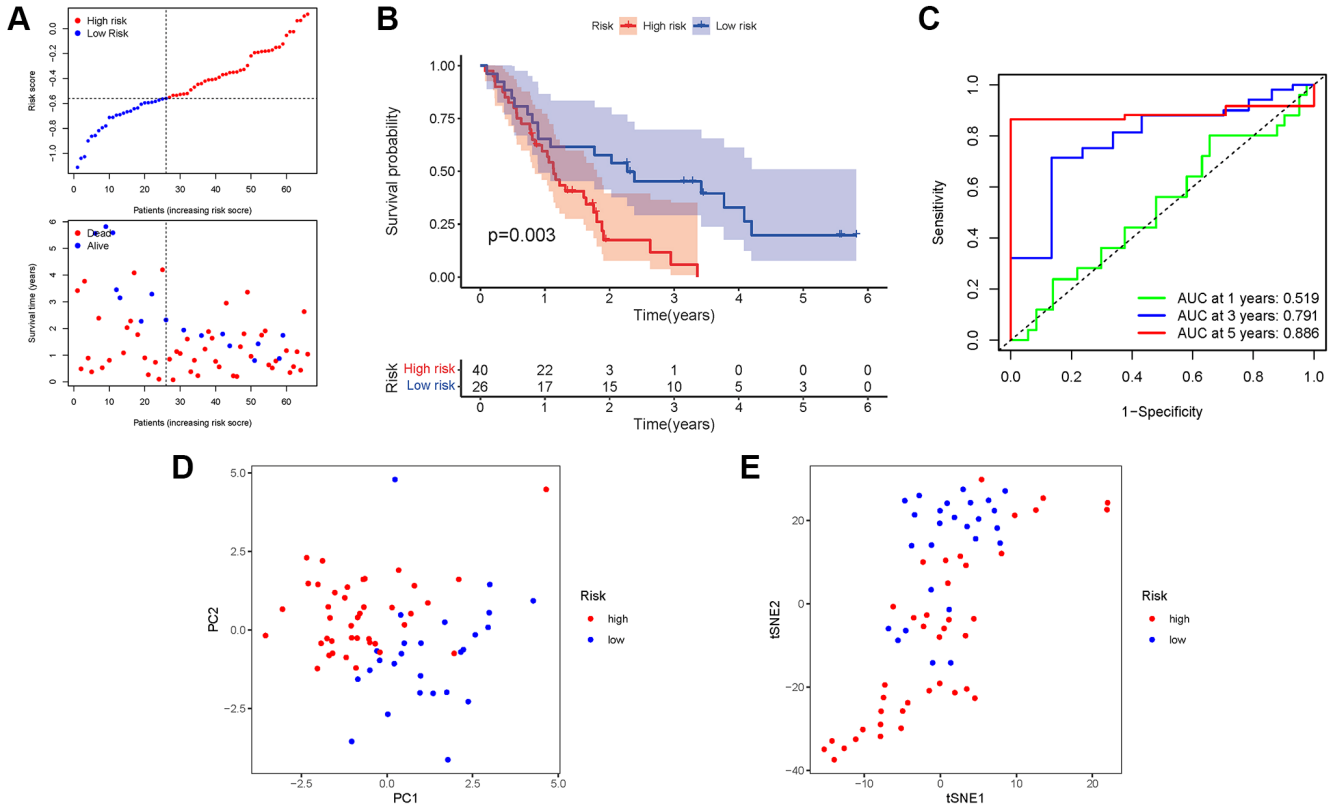

Figure 6. Validation of the risk model in the GEO cohort. (**A**) Risk survival status plot. (**B**) Kaplan–Meier curve result. (**C**) The AUC of the prediction of 1, 3, 5-year survival rate of PAAD. (**D**) PCA plot. (**E**) t-SNE plot.

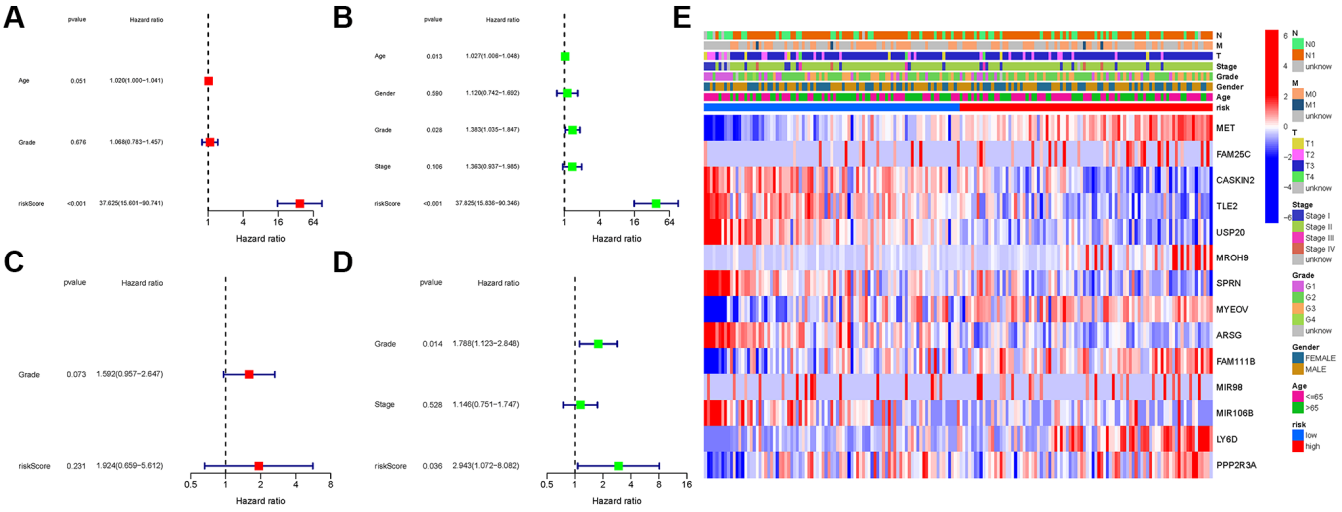

Figure 7. Univariate and multivariate cox regression analyses. (**A**, **B**) TCGA cohort. (**C**, **D**) GEO cohort. (**A**, **C**) Univariate analysis. (**B**, **D**) Multivariate analysis. (**E**) Heatmap.

conducted to investigate the involvement of essential targets and pathways in PAAD prognosis, resulting in the identification of a feasible biomarker and therapy target.

We found 25 DEGs associated with necroptosis, and the genes were divided into two groups to investigate their possible involvement in PAAD. Based on previous studies, NRGs were significantly linked to PAAD prognosis in a university Cox regression study. The researchers found that 14 prognostic NRGs were expressed differently in risk individuals. Some NRGs were found to be overexpressed in high-risk individuals ($P < 0.05$). In addition, we investigated the role of NRGs in PAAD. A survival study was used to measure the predictive value of NRGs. Patients with low-risk NRGs had longer life span. MET, AM25C, MROH9, MYEOV, FAM111B, Y6D, and PPP2R3A were highly expressed in the high-risk group, indicating that these genes may be related to the oncology process for patients with PAAD, and they seemed to be cancer-promoting genes. The results of the abovementioned genes provide some insights for further research, but conclusive evidence that they are involved in the expression of specific transcription factors related to necroptosis regulation, such as USP22, CDK9, and Foxo1 [24–26] is lacking, which requires further investigation. CASKIN2, TLE2, USP20, SPRN, ARSG, MIR106B, and MIR98 were considered to be substantially expressed in the low-risk group, suggesting that these genes may be PAAD tumor suppressor genes.

DATE truncation activated HGF expression in CRC cell lines, resulting in autocrine signaling via MET, thereby increasing cell proliferation and resistance to necroptosis. HGF signaling via MET decreased the levels of receptor-interacting serine-threonine kinase 1, a necroptosis mediator, in CRC cells [27]. MYEOV promotes pancreatic cancer progression by increasing HES1 expression and SOX9 transactivity [28]. The FAM111B gene mutation is linked to inherited exocrine pancreatic dysfunction [29]. TLE2 is linked to a good prognosis in pancreatic cancer, which regulates cell growth and gemcitabine sensitivity. These studies also demonstrate the validity and credibility of our findings

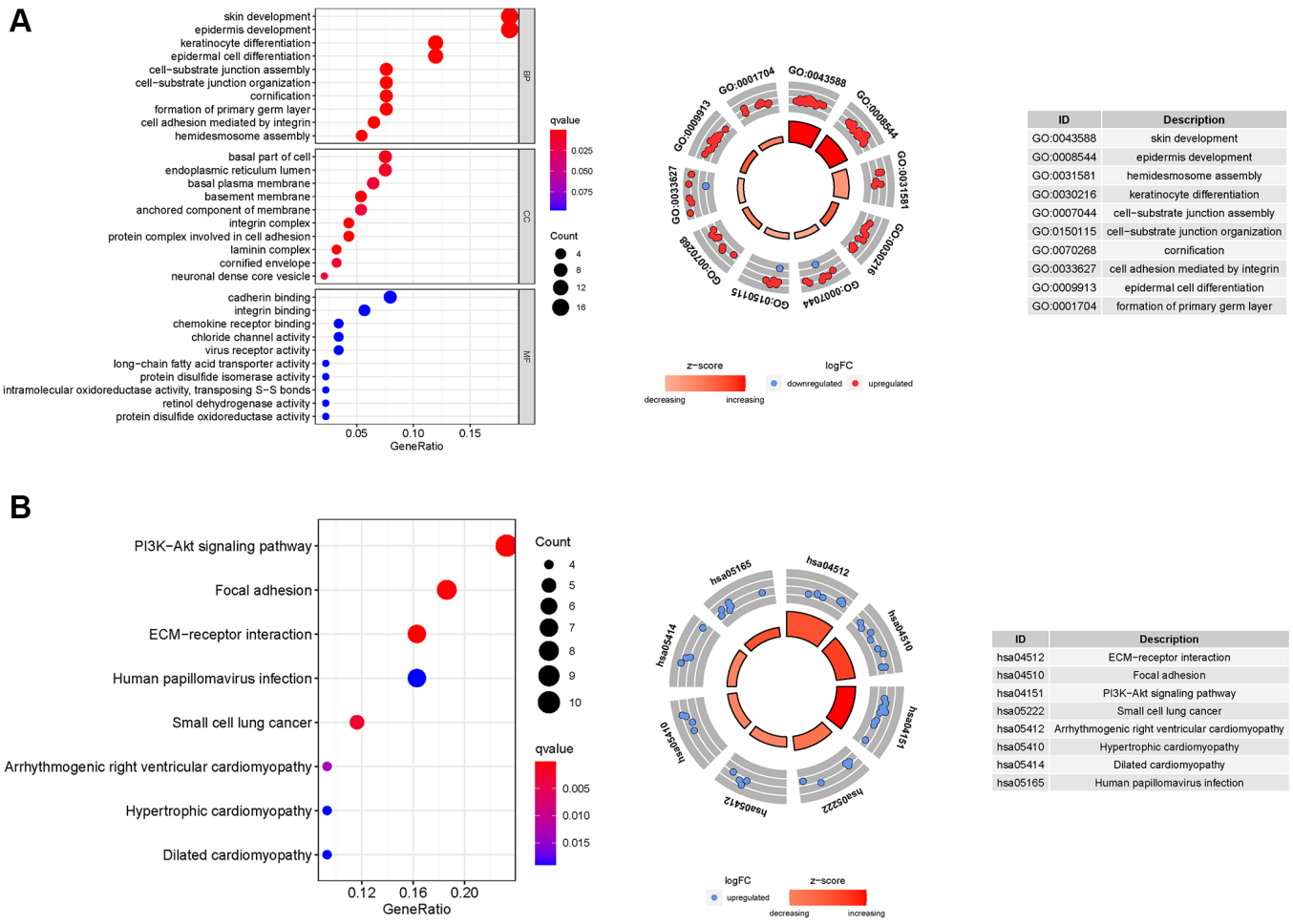

Figure 8. GO and KEGG analyses for ARGs. (**A**) GO, (**B**) KEGG.

[30]. The OS based on GSE62452 Kaplan-Meier curves and ROC analyses revealed that a necroptosis-related signature might be an independent prognostic predictor. Little research has been conducted on gene changes

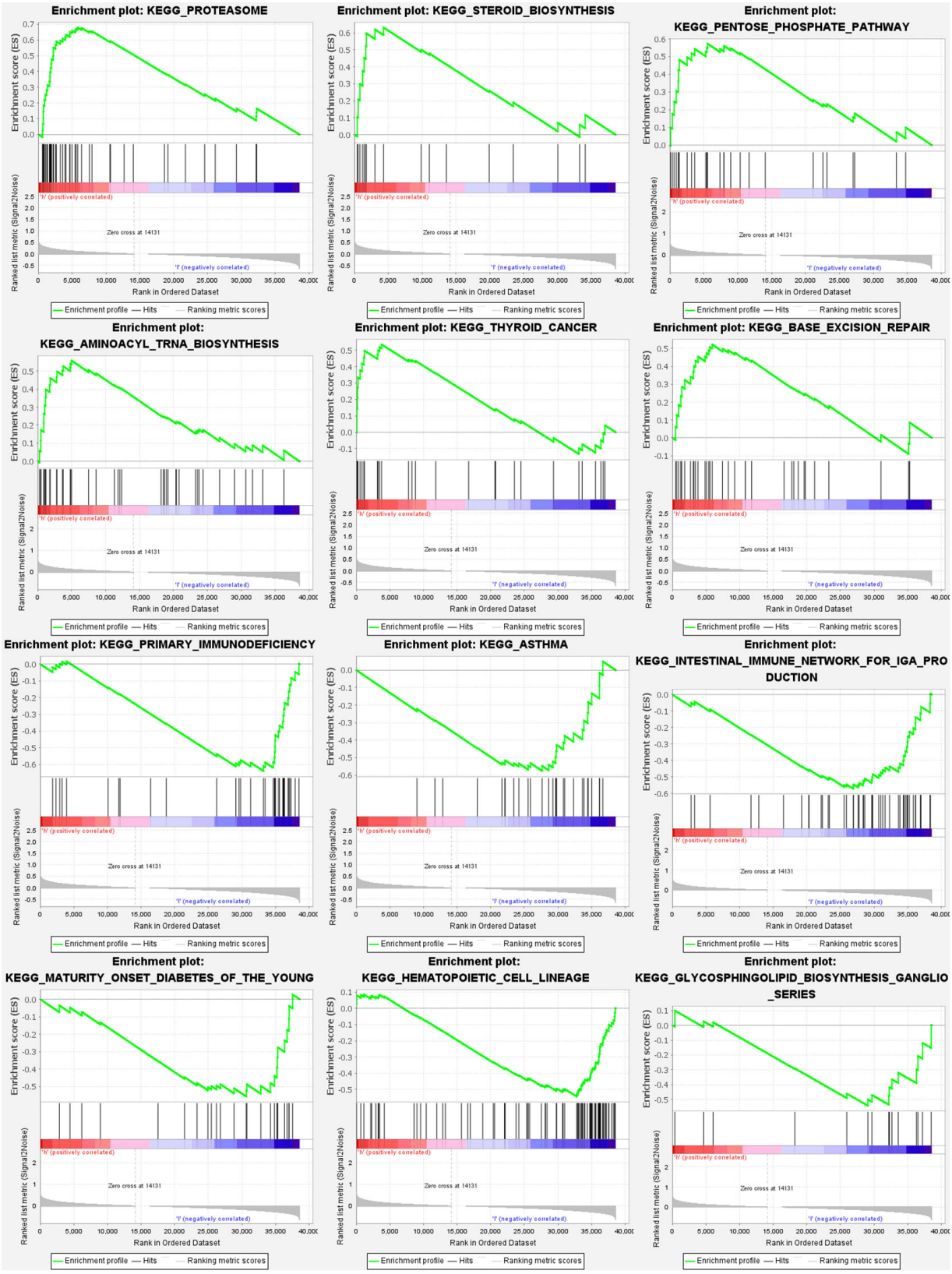

Figure 9. Gene set enrichment analyses.

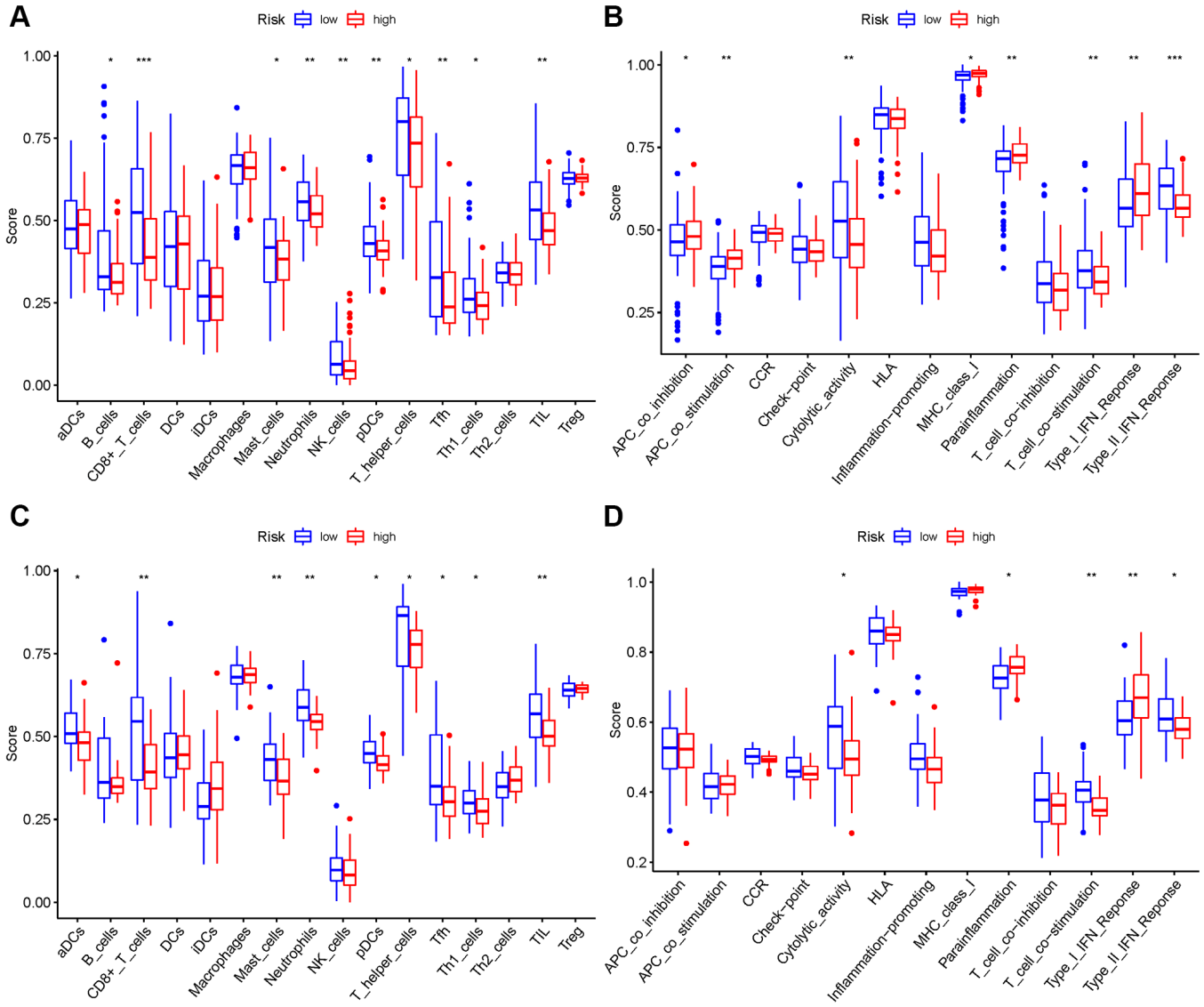

Figure 10. Comparison among ssGSEA scores. (**A**, **B**) TCGA cohort, (**C**, **D**) GEO cohort.

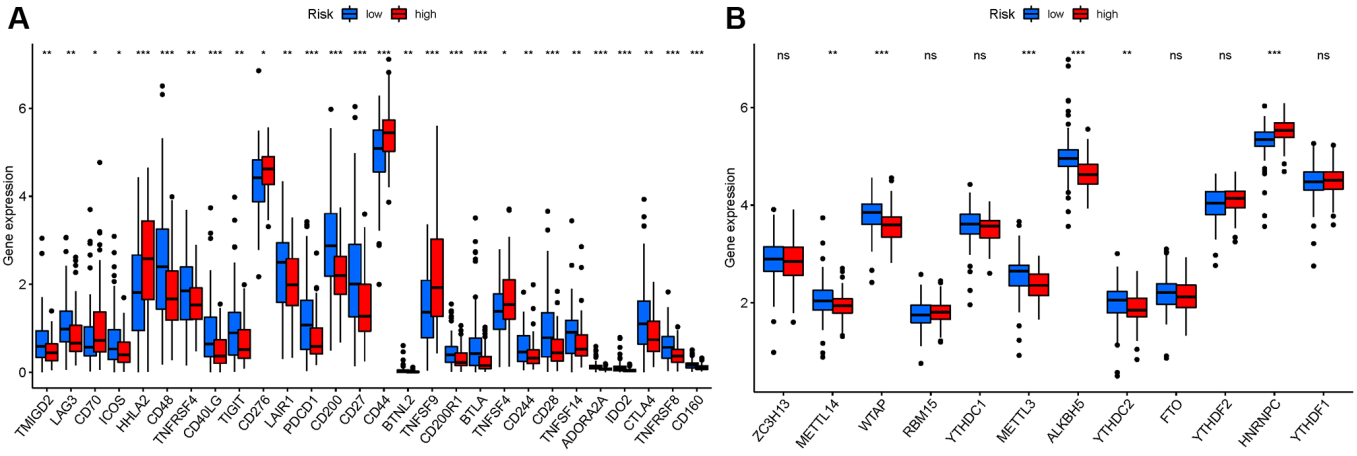

Figure 11. Analysis of the correlation of NRGs. (**A**) ICRGs in PAAD risk groups. (**B**) M6A-NRG in PAAD risk groups.

linked with necroptosis. Therefore, more research is needed to comprehend the mechanism of NRG change and fully identify and corroborate our findings.

In addition, KEGG analysis showed that NRGs were primarily involved in the PI3K-Akt signaling pathway. PI3K enhances tumor necrosis factor-induced necroptosis by activating the RIP1-RIP3-MLKL signaling pathway [31]. Consequently, necroptosis is crucial in PAAD. In GSEA, the p53 signaling pathway was the most significantly enriched pathway. A recent study has shown that p53 not only can cause necrosis via opening the mitochondrial permeability transition pore, but also can interact directly with cyclophilin D (CypD) to open the permeability transition pore (PTP) in the oxidative stress response [32]. *In vitro* and *in vivo* research has revealed that cyclin-dependent kinase inhibitor 3 (CDKN3) is adversely associated with pancreatic cancer tissue prognosis. CDKN3 can form a complex with MDM2-p53 to suppress the production of the P53 target gene P21, promoting the cell cycle and proliferation of PADD cells [33]. Considering the abovementioned criteria, NRGs may influence PAAD cell migration and proliferation via modulating the P53 signaling pathway.

Our method successfully predicts the survival of patients with PAAD. Based on the NRGs prognostic model, a rise in the risk score is associated with an increase in death and high-risk ratio. NRGs may be important biomarkers for predicting outcomes of patients with PAAD. Furthermore, we investigated and studied the relationship among NRGs, immune cells, immunological activity, immune checkpoints, and m6A. Recent research has found a link between various cell death mechanisms and antitumor immunity. Even in ICI-resistant tumors, pyroptosis, ferroptosis, and necroptosis activation combined with ICIs resulted in synergistically increased anticancer efficacy [34, 35]. An immunological checkpoint is the connection between SLC41A3 expression and immune cell invasion [36]. A microscopic investigation of the relationship among ICI, m6A, and pyrolysis has been conducted. Despite little analysis performed on NRGs and PAAD, supported by the abovementioned information, NRGs alterations were associated with the onset and development of PAAD.

Our research has limitations, although it is provided for theoretical underpinnings and research suggestions. First, we were unable to acquire sufficient external data from other publicly available sources to evaluate model's dependability. Second, we focused on signature of 14 risk-NRGs in our early expression study. However, no further functional or mechanistic research was conducted. Finally, no PAAD studies were conducted to confirm the link between prognostic genes and pyrolysis. Therefore, further research must be conducted to confirm the abovementioned findings.

CONCLUSIONS

A total of 14 anticipated NRGs were identified in patients with PAAD. The findings contributed to the comprehensive understanding of the relationship among necroptosis, immunological function, ICI, m6A, and immune cells, understanding the potential role of NRGs in the generation and development of PAAD malignant tumors, to provide research ideas for finding new therapeutic targets and prognostic indicators.

Abbreviations

PAAD: Pancreatic adenocarcinoma; GO: Gene ontology; AUC: Areas under the curve; MF: Molecular functions; ICIs: Immune checkpoint inhibitors; ROC: Receiver-operating characteristics; GSEA: Gene set enrichment analyses; TCGA: The Cancer Genome Atlas; NRGs: Necroptosis-related genes; BP: Biological processes; CC: Cellular components; OS: Overall survival; GEO: Gene Expression Omnibus; DEGs: Differentially expressed genes; KEGG: Kyoto Encyclopedia of Genes and Genomes.

AUTHOR CONTRIBUTIONS

Zixuan Wu drafted and revised the manuscript. Xuyan Huang and Minjie Cai were in charge of data collection. Peidong Huang conceived and designed this article, in charge of syntax modification, and revised the manuscript. Zunhui Guan revised the manuscript. All the authors have read and agreed to the final version of the manuscript.

ACKNOWLEDGMENTS

Thanks to Professor Huang for his strict guidance on this paper, and thanks to Miss Huang and Miss Cai for their support to this paper. Thanks to reviewers and editors for their sincere comments.

CONFLICTS OF INTEREST

The authors declare no conflicts of interest related to this study.

FUNDING

Health and Health Commission of Yunnan Province 2020 High-level TCM Reserve Talents Incubation Project (Yunwei TCM Development [2021] No. 1). The second round of construction project of The National Traditional

Chinese Medicine School Heritage Studio of the State Administration of Traditional Chinese Medicine (National Traditional Chinese Medicine Teaching Letter [2019] 62). Scientific and Technological Innovation Team of Acupuncture and Moxibustion Prevention and Treatment of Mental Disorders in Yunnan Colleges and Universities (No.: 2019YGC04).

REFERENCES

1. Katona BW, Brand RE, Canto MI, Chak A, Farrell JJ, Kastrinos F, Rustgi AK, Stoffel EM, Syngal S, Goggins M, and CAPS5 Study Consortium. Screening for Pancreatic Ductal Adenocarcinoma: Are We Asking the Impossible?-Letter. Cancer Prev Res (Phila). 2021; 14:973–4. https://doi.org/10.1158/1940-6207.CAPR-21-0233 PMID:34607877

2. Pasqualetti F, Sainato A, Morganti R, Laliscia C, Vasile E, Gonnelli A, Montrone S, Gadducci G, Giannini N, Coccia N, Fuentes T, Zanotti S, Falconi M, Paiar F. Adjuvant Radiotherapy in Patients With Pancreatic Adenocarcinoma. Is It Still Appealing in Clinical Trials? A Meta-analysis and Review of the Literature. Anticancer Res. 2021; 41:4697–704. https://doi.org/10.21873/anticanres.15283 PMID:34593417

3. Jin G, Ruan Q, Shangguan F, Lan L. RUNX2 and LAMC2: promising pancreatic cancer biomarkers identified by an integrative data mining of pancreatic adenocarcinoma tissues. Aging (Albany NY). 2021; 13:22963–84. https://doi.org/10.18632/aging.203589 PMID:34606473

4. Sordo-Bahamonde C, Lorenzo-Herrero S, Payer ÁR, Gonzalez S, López-Soto A. Mechanisms of Apoptosis Resistance to NK Cell-Mediated Cytotoxicity in Cancer. Int J Mol Sci. 2020; 21:3726. https://doi.org/10.3390/ijms21103726 PMID:32466293

5. Zhang P, Kawakami H, Liu W, Zeng X, Strebhardt K, Tao K, Huang S, Sinicrope FA. Targeting CDK1 and MEK/ERK Overcomes Apoptotic Resistance in BRAF-Mutant Human Colorectal Cancer. Mol Cancer Res. 2018; 16:378–89. https://doi.org/10.1158/1541-7786.MCR-17-0404 PMID:29233910

6. Chan VSH, Lam TPW, Lam WWM. Nephroptosis: The wandering kidney. Kidney Res Clin Pract. 2018; 37:306–7. https://doi.org/10.23876/j.krcp.2018.37.3.306 PMID:30254857

7. Degterev A, Hitomi J, Germscheid M, Ch'en IL, Korkina O, Teng X, Abbott D, Cuny GD, Yuan C, Wagner G, Hedrick SM, Gerber SA, Lugovskoy A, Yuan J. Identification of RIP1 kinase as a specific cellular target of necrostatins. Nat Chem Biol. 2008; 4:313–21. https://doi.org/10.1038/nchembio.83 PMID:18408713

8. Feng X, Song Q, Yu A, Tang H, Peng Z, Wang X. Receptor-interacting protein kinase 3 is a predictor of survival and plays a tumor suppressive role in colorectal cancer. Neoplasma. 2015; 62:592–601. https://doi.org/10.4149/neo_2015_071 PMID:25997957

9. Höckendorf U, Yabal M, Herold T, Munkhbaatar E, Rott S, Jilg S, Kauschinger J, Magnani G, Reisinger F, Heuser M, Kreipe H, Sotlar K, Engleitner T, et al. RIPK3 Restricts Myeloid Leukemogenesis by Promoting Cell Death and Differentiation of Leukemia Initiating Cells. Cancer Cell. 2016; 30:75–91. https://doi.org/10.1016/j.ccell.2016.06.002 PMID:27411587

10. Seifert L, Werba G, Tiwari S, Giao Ly NN, Alothman S, Alqunaibit D, Avanzi A, Barilla R, Daley D, Greco SH, Torres-Hernandez A, Pergamo M, Ochi A, et al. The necrosome promotes pancreatic oncogenesis via CXCL1 and Mincle-induced immune suppression. Nature. 2016; 532:245–9. https://doi.org/10.1038/nature17403 PMID:27049944

11. Krysko O, Aaes TL, Kagan VE, D'Herde K, Bachert C, Leybaert L, Vandenabeele P, Krysko DV. Necroptotic cell death in anti-cancer therapy. Immunol Rev. 2017; 280:207–19. https://doi.org/10.1111/imr.12583 PMID:29027225

12. Yan J, Wan P, Choksi S, Liu ZG. Necroptosis and tumor progression. Trends Cancer. 2022; 8:21–7. https://doi.org/10.1016/j.trecan.2021.09.003 PMID:34627742

13. Zhao E, Chen S, Dang Y. Development and External Validation of a Novel Immune Checkpoint-Related Gene Signature for Prediction of Overall Survival in Hepatocellular Carcinoma. Front Mol Biosci. 2021; 7:620765. https://doi.org/10.3389/fmolb.2020.620765 PMID:33553243

14. Ye Y, Dai Q, Qi H. A novel defined pyroptosis-related gene signature for predicting the prognosis of ovarian cancer. Cell Death Discov. 2021; 7:71. https://doi.org/10.1038/s41420-021-00451-x PMID:33828074

15. Wang Z, Jensen MA, Zenklusen JC. A Practical Guide to The Cancer Genome Atlas (TCGA). Methods Mol Biol. 2016; 1418:111–41.

https://doi.org/10.1007/978-1-4939-3578-9_6
PMID:27008012

16. Yu ZL, Zhu ZM. Comprehensive analysis of N6-methyladenosine -related long non-coding RNAs and immune cell infiltration in hepatocellular carcinoma. Bioengineered. 2021; 12:1708–24. https://doi.org/10.1080/21655979.2021.1923381 PMID:33955330

17. Wu P, Heins ZJ, Muller JT, Katsnelson L, de Bruijn I, Abeshouse AA, Schultz N, Fenyö D, Gao J. Integration and Analysis of CPTAC Proteomics Data in the Context of Cancer Genomics in the cBioPortal. Mol Cell Proteomics. 2019; 18:1893–8. https://doi.org/10.1074/mcp.TIR119.001673 PMID:31308250

18. David CC, Jacobs DJ. Principal component analysis: a method for determining the essential dynamics of proteins. Methods Mol Biol. 2014; 1084:193–226. https://doi.org/10.1007/978-1-62703-658-0_11 PMID:24061923

19. Tang Y, Li C, Zhang YJ, Wu ZH. Ferroptosis-Related Long Non-Coding RNA signature predicts the prognosis of Head and neck squamous cell carcinoma. Int J Biol Sci. 2021; 17:702–11. https://doi.org/10.7150/ijbs.55552 PMID:33767582

20. Lambert A, Schwarz L, Ducreux M, Conroy T. Neoadjuvant Treatment Strategies in Resectable Pancreatic Cancer. Cancers (Basel). 2021; 13:4724. https://doi.org/10.3390/cancers13184724 PMID:34572951

21. Kowalski S, Hać S, Wyrzykowski D, Zauszkiewicz-Pawlak A, Inkielewicz-Stępniak I. Selective cytotoxicity of vanadium complexes on human pancreatic ductal adenocarcinoma cell line by inducing necroptosis, apoptosis and mitotic catastrophe process. Oncotarget. 2017; 8:60324–41. https://doi.org/10.18632/oncotarget.19454 PMID:28947974

22. Erkes DA, Cai W, Sanchez IM, Purwin TJ, Rogers C, Field CO, Berger AC, Hartsough EJ, Rodeck U, Alnemri ES, Aplin AE. Mutant BRAF and MEK Inhibitors Regulate the Tumor Immune Microenvironment via Pyroptosis. Cancer Discov. 2020; 10:254–69. https://doi.org/10.1158/2159-8290.CD-19-0672 PMID:31796433

23. Hou J, Zhao R, Xia W, Chang CW, You Y, Hsu JM, Nie L, Chen Y, Wang YC, Liu C, Wang WJ, Wu Y, Ke B, et al. Author Correction: PD-L1-mediated gasdermin C expression switches apoptosis to pyroptosis in cancer cells and facilitates tumour necrosis. Nat Cell Biol. 2020; 22:1396. https://doi.org/10.1038/s41556-020-00599-1 PMID:33033376

24. Roedig J, Kowald L, Juretschke T, Karlowitz R, Ahangarian Abhari B, Roedig H, Fulda S, Beli P, van Wijk SJ. USP22 controls necroptosis by regulating receptor-interacting protein kinase 3 ubiquitination. EMBO Rep. 2021; 22:e50163. https://doi.org/10.15252/embr.202050163 PMID:33369872

25. Li J, Shi J, Pan Y, Zhao Y, Yan F, Li H, Lei L. Transcription modulation by CDK9 regulates inflammatory genes and RIPK3-MLKL-mediated necroptosis in periodontitis progression. Sci Rep. 2019; 9:17369. https://doi.org/10.1038/s41598-019-53910-y PMID:31758083

26. Li C, Sheng M, Lin Y, Xu D, Tian Y, Zhan Y, Jiang L, Coito AJ, Busuttil RW, Farmer DG, Kupiec-Weglinski JW, Ke B. Functional crosstalk between myeloid Foxo1-β-catenin axis and Hedgehog/Gli1 signaling in oxidative stress response. Cell Death Differ. 2021; 28:1705–19. https://doi.org/10.1038/s41418-020-00695-7 PMID:33288903

27. Seneviratne D, Ma J, Tan X, Kwon YK, Muhammad E, Melhem M, DeFrances MC, Zarnegar R. Genomic instability causes HGF gene activation in colon cancer cells, promoting their resistance to necroptosis. Gastroenterology. 2015; 148:181–91.e17. https://doi.org/10.1053/j.gastro.2014.09.019 PMID:25244939

28. Liang E, Lu Y, Shi Y, Zhou Q, Zhi F. MYEOV increases HES1 expression and promotes pancreatic cancer progression by enhancing SOX9 transactivity. Oncogene. 2020; 39:6437–50. https://doi.org/10.1038/s41388-020-01443-4 PMID:32879444

29. Seo A, Walsh T, Lee MK, Ho PA, Hsu EK, Sidbury R, King MC, Shimamura A. FAM111B Mutation Is Associated With Inherited Exocrine Pancreatic Dysfunction. Pancreas. 2016; 45:858–62. https://doi.org/10.1097/MPA.0000000000000529 PMID:26495788

30. Hu S, Chen Z, Gu J, Tan L, Zhang M, Lin W. TLE2 is associated with favorable prognosis and regulates cell growth and gemcitabine sensitivity in pancreatic cancer. Ann Transl Med. 2020; 8:1017. https://doi.org/10.21037/atm-20-5492 PMID:32953817

31. Hu S, Chang X, Zhu H, Wang D, Chen G. PI3K mediates tumor necrosis factor induced-necroptosis through initiating RIP1-RIP3-MLKL signaling pathway activation. Cytokine. 2020; 129:155046.

https://doi.org/10.1016/j.cyto.2020.155046
PMID:32114297

32. Garancher A, Suzuki H, Haricharan S, Chau LQ, Masihi MB, Rusert JM, Norris PS, Carrette F, Romero MM, Morrissy SA, Skowron P, Cavalli FMG, Farooq H, et al. Tumor necrosis factor overcomes immune evasion in p53-mutant medulloblastoma. Nat Neurosci. 2020; 23:842–53.
https://doi.org/10.1038/s41593-020-0628-4
PMID:32424282 Retraction in: Nat Neurosci. 2022; 25:127.
https://doi.org/10.1038/s41593-021-00994-3
PMID:34907396

33. Liu D, Zhang J, Wu Y, Shi G, Yuan H, Lu Z, Zhu Q, Wu P, Lu C, Guo F, Chen J, Jiang K, Miao Y. YY1 suppresses proliferation and migration of pancreatic ductal adenocarcinoma by regulating the CDKN3/MdM2/P53/P21 signaling pathway. Int J Cancer. 2018; 142:1392–404.
https://doi.org/10.1002/ijc.31173
PMID:29168185

34. Tang R, Xu J, Zhang B, Liu J, Liang C, Hua J, Meng Q, Yu X, Shi S. Ferroptosis, necroptosis, and pyroptosis in anticancer immunity. J Hematol Oncol. 2020; 13:110.
https://doi.org/10.1186/s13045-020-00946-7
PMID:32778143

35. Hsu SK, Li CY, Lin IL, Syue WJ, Chen YF, Cheng KC, Teng YN, Lin YH, Yen CH, Chiu CC. Inflammation-related pyroptosis, a novel programmed cell death pathway, and its crosstalk with immune therapy in cancer treatment. Theranostics. 2021; 11:8813–35.
https://doi.org/10.7150/thno.62521
PMID:34522213

36. Liu J, Zhang S, Dai W, Xie C, Li JC. A Comprehensive Prognostic and Immune Analysis of SLC41A3 in Pan-Cancer. Front Oncol. 2021; 10:586414.
https://doi.org/10.3389/fonc.2020.586414
PMID:33520701

SUPPLEMENTARY MATERIALS

Supplementary Tables

Supplementary Table 1. 52 necroptosis-related genes.

BAK1	CHMP4B	IL18	CASP9	NLRP6
BAX	CHMP4C	IL1A	GPX4	NLRP7
CASP1	CHMP6	IL1B	GSDMA	NOD1
CASP3	CHMP7	IRF1	GSDMB	NOD2
CASP4	CYCS	IRF2	GSDMC	PJVK
CASP5	ELANE	TP53	IL6	PLCG1
CHMP2A	GSDMD	TP63	NLRC4	PRKACA
CHMP2B	GSDME	AIM2	NLRP1	PYCARD
CHMP3	GZMB	CASP6	NLRP2	SCAF11
CHMP4A	HMGB1	CASP8	NLRP3	TIRAP
TNF	GZMA			

Supplementary Table 2. 25 DEGs linked to NRGs.

gene	conMean	treatMean	logFC	*p* Value
TNF	2.9597148	0.878954778	−1.751597318	0.023229673
CYBB	44.8476025	13.38835502	−1.74405215	0.004999667
SLC25A6	260.2667	212.1314808	−0.295032001	0.029730049
PYGB	26.3985825	75.0233836	1.506879866	0.002884394
PLA2G4C	3.36357325	1.527573251	−1.138753114	0.007311847
PLA2G4F	0.096944548	0.69805447	2.848107951	0.01144699
CAPN2	29.2810825	50.60433046	0.789291959	0.012420784
NLRP3	2.307436	1.149735351	−1.004988816	0.014207465
RNF103-CHMP3	0.03308378	0.125159531	1.919572176	0.049686083
CHMP4C	7.25279525	14.30096114	0.979503084	0.038630253
FASLG	1.15240325	0.348416184	−1.725762088	0.037736936
IFNA2	0.012599015	0.001135769	−3.471569966	0.000288726
IFNA6	0.021787193	0.001020912	−4.415549216	0.000203649
IFNA13	0.00733201	0.001187969	−2.625711059	0.001901453
IFNGR1	67.564385	40.74547212	−0.729623216	0.009433631
JAK1	49.8170925	34.40897001	−0.533856116	0.044375834
JAK3	12.6223675	4.252687198	−1.569535885	0.019953735
TYK2	19.87963	12.60590665	−0.657191021	0.048594059
STAT4	3.619687	1.434699334	−1.335116524	0.03600294
STAT5A	14.5681125	9.021417197	−0.691387976	0.017539418
TLR4	7.0368955	3.415832457	−1.042701875	0.021537533
TNFAIP3	30.580245	13.05847187	−1.227613886	0.002033049
H2AW	3.70185	10.68664761	1.529491009	0.024420867
H2AC6	10.024392	27.38610677	1.449929449	0.015385115
BCL2	7.155259	2.040894169	−1.809802617	0.014983353

Supplementary Table 3. Hub genes.

Name	Betweenness	Closeness	Degree	Network
JAK1	58.62251082	0.296875	11	9.223809524
TNF	30.05974026	0.287878788	11	9.555555556
JAK3	42.26688312	0.292307692	10	8.103174603
IFNGR1	20.94393939	0.28358209	10	8.158730159
TLR4	32.18744589	0.28358209	10	8.357142857
TYK2	13.49307359	0.28358209	10	8.583333333
STAT4	5.093073593	0.275362319	8	6.726190476
STAT5A	13.33333333	0.271428571	7	5.833333333
IFNA2	0.6	0.263888889	6	5.8
IFNA6	0	0.256756757	5	5
TNFAIP3	1.533333333	0.25	5	4.166666667
CYBB	1.2	0.25	4	3.333333333
NLRP3	0.666666667	0.243589744	4	3.333333333
BCL2	60	0.253333333	3	1
IFNA13	0	0.246753247	3	3
HIST1H2AC	32	0.213483146	2	0
FASLG	0	0.234567901	2	2
CHMP3	0	0.052631579	1	0
CHMP4C	0	0.052631579	1	0
HIST3H2A	0	0.180952381	1	0

Supplementary Table 4. 14 risk PRGs.

Id	TCGA-3A-A9J0	TCGA-2L-AAQL	TCGA-US-A77E	TCGA-RB-AA9M
MET	5.042611	4.7215981	5.9641271	5.2955498
FAM25C	2.0205815	2.2528105	2.0205815	2.0205815
CASKIN2	4.1749081	3.58593	4.0714195	4.1428019
TLE2	4.1259097	4.624045	3.999072	4.7286858
USP20	3.0161423	3.715024	3.7000295	3.641327
MROH9	1.0486983	0.9140702	0.9140702	0.9350862
SPRN	2.6244162	2.8517601	2.3841645	2.6025939
MYEOV	3.2386553	4.1509198	4.4052511	3.667548
ARSG	2.2785722	2.0642247	2.3422646	2.3341557
FAM111B	2.6997762	1.4177758	1.9956956	2.4969894
MIR98	0.8402696	1.218496	1.1183522	0.8402696
MIR106B	2.7306465	1.4784037	1.4784037	2.6675028
LY6D	1.9197985	2.4401492	2.8759444	5.8630146
PPP2R3A	2.3522622	2.2616753	2.9258627	3.446074
riskScore	−0.847267824	−0.659885519	−0.580465013	−0.643074732
risk	low	low	low	low

Supplementary Table 5A. GO enrichment analysis.

Ontology	Description	BgRatio	*p* value	*q* value
BP	skin development	415/18862	1.49E-11	2.35E-08
BP	epidermis development	463/18862	8.27E-11	6.50E-08
BP	hemidesmosome assembly	12/18862	1.91E-09	9.99E-07
BP	keratinocyte differentiation	302/18862	2.51E-07	9.88E-05
BP	cell-substrate junction assembly	100/18862	5.77E-07	0.000181471
BP	cell-substrate junction organization	106/18862	8.58E-07	0.00021942
BP	cornification	113/18862	1.32E-06	0.00021942
BP	cell adhesion mediated by integrin	72/18862	1.38E-06	0.00021942
BP	epidermal cell differentiation	360/18862	1.42E-06	0.00021942
BP	formation of primary germ layer	115/18862	1.49E-06	0.00021942
BP	keratinization	225/18862	1.53E-06	0.00021942
BP	cell-matrix adhesion	230/18862	1.84E-06	0.000241166
BP	gastrulation	179/18862	2.66E-06	0.000321238
BP	extracellular matrix organization	393/18862	3.31E-06	0.000350118
BP	extracellular structure organization	394/18862	3.39E-06	0.000350118
BP	external encapsulating structure organization	396/18862	3.56E-06	0.000350118
BP	cell-substrate adhesion	359/18862	9.94E-06	0.000919336
BP	mesodermal cell differentiation	32/18862	1.72E-05	0.001499725
BP	mesoderm formation	68/18862	2.02E-05	0.001674835
BP	mesoderm morphogenesis	70/18862	2.33E-05	0.001833235
BP	positive regulation of chemotaxis	139/18862	6.09E-05	0.004395847
BP	epithelial cell migration	357/18862	6.15E-05	0.004395847
BP	epithelium migration	360/18862	6.56E-05	0.004483738
BP	negative regulation of anoikis	17/18862	7.27E-05	0.004584778
BP	tissue migration	365/18862	7.29E-05	0.004584778
BP	keratinocyte proliferation	48/18862	8.75E-05	0.005293053
BP	ameboidal-type cell migration	473/18862	0.000102639	0.005822652
BP	entry into host	153/18862	0.00010367	0.005822652
BP	integrin-mediated signaling pathway	106/18862	0.000170071	0.009222742
BP	response to prostaglandin E	23/18862	0.000185292	0.009713186
BP	establishment of skin barrier	24/18862	0.000211015	0.010283511
BP	regulation of anoikis	24/18862	0.000211015	0.010283511
BP	movement in host environment	175/18862	0.000215789	0.010283511
BP	cell junction assembly	425/18862	0.00022915	0.010599087
BP	regulation of water loss via skin	26/18862	0.00026916	0.012093978
BP	positive regulation of cell projection organization	344/18862	0.000277513	0.012122947
BP	positive regulation of granulocyte chemotaxis	27/18862	0.000301738	0.012824934
BP	mesoderm development	123/18862	0.0003398	0.014062637
BP	response to prostaglandin	30/18862	0.000414413	0.016710737
BP	anoikis	34/18862	0.000602246	0.023677781
BP	biological process involved in interaction with host	219/18862	0.000710972	0.027270667
BP	cell chemotaxis	306/18862	0.000745332	0.027907915
BP	regulation of keratinocyte proliferation	37/18862	0.000773772	0.028299038
BP	regulation of chemotaxis	224/18862	0.000799698	0.028582522
BP	bone remodeling	89/18862	0.000943054	0.03295725
BP	regulation of dopaminergic neuron differentiation	10/18862	0.001032363	0.035294066
BP	epithelial cell proliferation	428/18862	0.00116202	0.038038774
BP	regulation of dendritic cell antigen processing and presentation	11/18862	0.001257775	0.038038774
BP	protein folding in endoplasmic reticulum	11/18862	0.001257775	0.038038774
BP	skin morphogenesis	11/18862	0.001257775	0.038038774
BP	dendritic cell apoptotic process	11/18862	0.001257775	0.038038774
BP	regulation of dendritic cell apoptotic process	11/18862	0.001257775	0.038038774
BP	endodermal cell differentiation	44/18862	0.001286801	0.038182347

BP	brown fat cell differentiation	46/18862	0.001464569	0.04265236
BP	establishment of T cell polarity	12/18862	0.001504544	0.043019868
BP	regulation of cell adhesion mediated by integrin	48/18862	0.001657031	0.04570258
BP	tissue homeostasis	260/18862	0.001717022	0.04570258
BP	regulation of granulocyte chemotaxis	49/18862	0.001758907	0.04570258
BP	establishment of lymphocyte polarity	13/18862	0.001772461	0.04570258
BP	immunological synapse formation	13/18862	0.001772461	0.04570258
BP	regulation of insulin secretion	178/18862	0.001794325	0.04570258
BP	positive regulation of plasma membrane bounded cell projection assembly	106/18862	0.001801795	0.04570258
BP	regulation of bone remodeling	51/18862	0.001974208	0.049280987
CC	integrin complex	31/19520	1.38E-05	0.000958944
CC	laminin complex	12/19520	2.23E-05	0.000958944
CC	protein complex involved in cell adhesion	36/19520	2.53E-05	0.000958944
CC	basement membrane	94/19520	8.65E-05	0.002459337
CC	basal part of cell	258/19520	0.000233992	0.005320244
CC	endoplasmic reticulum lumen	306/19520	0.000650914	0.012333107
CC	basal plasma membrane	240/19520	0.001014444	0.016475178
CC	cornified envelope	45/19520	0.001285224	0.016721371
CC	anchored component of membrane	170/19520	0.001323775	0.016721371
CC	neuronal dense core vesicle	13/19520	0.001692709	0.019243428
CC	costamere	18/19520	0.003269266	0.033787629
CC	intermediate filament	215/19520	0.00366975	0.034766056
CC	cell-substrate junction	423/19520	0.004089977	0.035766605
CC	lamellipodium membrane	22/19520	0.004875244	0.039588448
CC	cortical actin cytoskeleton	78/19520	0.006154032	0.045305642
CC	apical plasma membrane	351/19520	0.006659117	0.045305642
CC	microvillus membrane	26/19520	0.006774871	0.045305642
CC	intermediate filament cytoskeleton	256/19520	0.007604382	0.046857122
CC	dense core granule	28/19520	0.007831213	0.046857122
CC	cell-cell junction	485/19520	0.008465165	0.04811778

Supplementary Table 5B. KEGG enrichment analysis.

ID	Description	BgRatio	*p* value	*q* value
hsa04512	ECM-receptor interaction	88/8105	3.28E-07	3.11E-05
hsa04510	Focal adhesion	201/8105	8.56E-06	0.000370605
hsa04151	PI3K-Akt signaling pathway	354/8105	1.17E-05	0.000370605
hsa05222	Small cell lung cancer	92/8105	0.00011567	0.002739557
hsa05412	Arrhythmogenic right ventricular cardiomyopathy	77/8105	0.000701775	0.01329678
hsa05410	Hypertrophic cardiomyopathy	90/8105	0.001260558	0.019074857
hsa05414	Dilated cardiomyopathy	96/8105	0.001601543	0.019074857
hsa05165	Human papillomavirus infection	331/8105	0.001610766	0.019074857

Supplementary Table 6A. GSEA of high risk.

NAME	ES	NES	NOM *p*-val	FDR *q*-val
KEGG_PENTOSE_PHOSPHATE_PATHWAY	0.5729152	1.6310743	0.01953125	1
KEGG_PROTEASOME	0.6784165	1.6303458	0.049701788	0.6821798
KEGG_GLYCOSPHINGOLIPID_BIOSYNTHESIS_LACTO_AND_NEOLACTO_SERIES	0.5090886	1.5907345	0.024952015	0.6408247
KEGG_THYROID_CANCER	0.53489053	1.5439887	0.05179283	0.6907832
KEGG_P53_SIGNALING_PATHWAY	0.47881857	1.5324117	0.04347826	0.60003185
KEGG_GLYCOLYSIS_GLUCONEOGENESIS	0.47841245	1.5322174	0.037698414	0.50075066
KEGG_ADHERENS_JUNCTION	0.4795818	1.5175084	0.0662768	0.47806197
KEGG_STEROID_BIOSYNTHESIS	0.6314558	1.4914162	0.09486166	0.4986435
KEGG_PATHOGENIC_ESCHERICHIA_COLI_INFECTION	0.48299125	1.4645706	0.086105675	0.524178
KEGG_TIGHT_JUNCTION	0.39693546	1.4420464	0.063872255	0.54062873
KEGG_AMINOACYL_TRNA_BIOSYNTHESIS	0.5580433	1.4407	0.11516315	0.49625063
KEGG_STARCH_AND_SUCROSE_METABOLISM	0.46116272	1.4073405	0.08583691	0.5482185
KEGG_GALACTOSE_METABOLISM	0.48794708	1.3951346	0.091617934	0.53853256
KEGG_CELL_CYCLE	0.4647909	1.3540881	0.19960861	0.61424387
KEGG_AXON_GUIDANCE	0.3714874	1.3263278	0.10852713	0.6551905
KEGG_BASE_EXCISION_REPAIR	0.5224427	1.3245112	0.1809145	0.6192906
KEGG_O_GLYCAN_BIOSYNTHESIS	0.45017973	1.321248	0.1764706	0.5923887
KEGG_PORPHYRIN_AND_CHLOROPHYLL_METABOLISM	0.42830938	1.3130741	0.13465346	0.5810344
KEGG_GLYCOSAMINOGLYCAN_BIOSYNTHESIS_KERATAN_SULFATE	0.48650512	1.3112824	0.13765182	0.55493397
KEGG_PENTOSE_AND_GLUCURONATE_INTERCONVERSIONS	0.46371907	1.2722654	0.18218623	0.62946343
KEGG_BLADDER_CANCER	0.39896894	1.256486	0.18992248	0.6436727
KEGG_REGULATION_OF_ACTIN_CYTOSKELETON	0.33413285	1.250563	0.17105263	0.62979627
KEGG_PANCREATIC_CANCER	0.39570457	1.2432532	0.22896282	0.6211923
KEGG_PATHWAYS_IN_CANCER	0.33537713	1.2430347	0.17017208	0.59580684
KEGG_DRUG_METABOLISM_OTHER_ENZYMES	0.40908697	1.2375876	0.1609658	0.58401114
KEGG_SMALL_CELL_LUNG_CANCER	0.3896531	1.2231851	0.22178218	0.59402245
KEGG_ENDOCYTOSIS	0.3299927	1.2194865	0.20610687	0.58074325
KEGG_ONE_CARBON_POOL_BY_FOLATE	0.47091427	1.2165351	0.256167	0.5663879
KEGG_AMINO_SUGAR_AND_NUCLEOTIDE_SUGAR_METABOLISM	0.4007442	1.2126254	0.23745173	0.55516595
KEGG_N_GLYCAN_BIOSYNTHESIS	0.40781587	1.2106607	0.23287672	0.5410943
KEGG_ASCORBATE_AND_ALDARATE_METABOLISM	0.45372823	1.2069958	0.2371134	0.530202
KEGG_DNA_REPLICATION	0.50567645	1.1796668	0.35166994	0.56995404
KEGG_OOCYTE_MEIOSIS	0.36010596	1.1793286	0.26061776	0.55347526
KEGG_SYSTEMIC_LUPUS_ERYTHEMATOSUS	0.37165263	1.1768961	0.25851703	0.54163045
KEGG_FRUCTOSE_AND_MANNOSE_METABOLISM	0.39953077	1.1730746	0.29766536	0.53443813
KEGG_ARRHYTHMOGENIC_RIGHT_VENTRICULAR_CARDIOMYOPATHY_ARVC	0.35322598	1.1730168	0.26061776	0.5197308
KEGG_FOCAL_ADHESION	0.34690592	1.1704245	0.2751938	0.51039374
KEGG_MISMATCH_REPAIR	0.4998743	1.1677153	0.3300199	0.50204176
KEGG_NOTCH_SIGNALING_PATHWAY	0.35844958	1.1651915	0.25581396	0.49362785
KEGG_ECM_RECEPTOR_INTERACTION	0.38675836	1.1465491	0.3151751	0.51444507
KEGG_PYRIMIDINE_METABOLISM	0.35571525	1.1058619	0.34740883	0.5765829
KEGG_STEROID_HORMONE_BIOSYNTHESIS	0.33638063	1.0779973	0.34631148	0.6170261
KEGG_BIOSYNTHESIS_OF_UNSATURATED_FATTY_ACIDS	0.39363536	1.0769395	0.35416666	0.60520357
KEGG_ENDOMETRIAL_CANCER	0.3395971	1.0718687	0.40151516	0.60124856
KEGG_GLUTATHIONE_METABOLISM	0.32758725	1.0697683	0.35	0.5916402
KEGG_HOMOLOGOUS_RECOMBINATION	0.42976084	1.0597887	0.44646466	0.59751785
KEGG_BASAL_CELL_CARCINOMA	0.32655776	1.0506406	0.38491297	0.6011576
KEGG_CHRONIC_MYELOID_LEUKEMIA	0.33301565	1.0484524	0.4165067	0.5925686
KEGG_WNT_SIGNALING_PATHWAY	0.2844261	1.0387905	0.39961758	0.598086
KEGG_NUCLEOTIDE_EXCISION_REPAIR	0.37913045	1.0309824	0.44656488	0.60022134
KEGG_RENAL_CELL_CARCINOMA	0.3186963	1.0266781	0.41917294	0.59651726
KEGG_SPLICEOSOME	0.36476433	1.0200957	0.4743833	0.5970973

KEGG_PROSTATE_CANCER	0.30396676	1.0045717	0.433526	0.6138756
KEGG_METABOLISM_OF_XENOBIOTICS_BY_CYTOCHROME_P450	0.31419396	0.9750271	0.4947589	0.6572137
KEGG_UBIQUITIN_MEDIATED_PROTEOLYSIS	0.30457303	0.9725739	0.4952199	0.6495022
KEGG_APOPTOSIS	0.30550128	0.9666593	0.5116279	0.6480138
KEGG_HYPERTROPHIC_CARDIOMYOPATHY_HCM	0.2806289	0.9614698	0.5190381	0.6459331
KEGG_VEGF_SIGNALING_PATHWAY	0.27282158	0.9604114	0.5095785	0.63673884
KEGG_RNA_DEGRADATION	0.3311516	0.95151705	0.54285717	0.641828
KEGG_ALZHEIMERS_DISEASE	0.30191407	0.9506232	0.5248509	0.632659
KEGG_RETINOL_METABOLISM	0.3078011	0.93862295	0.53503186	0.6427308
KEGG_ETHER_LIPID_METABOLISM	0.2848933	0.92489564	0.5694165	0.65457636
KEGG_MELANOMA	0.25767887	0.9193458	0.5755814	0.65356475
KEGG_COLORECTAL_CANCER	0.28481606	0.9170352	0.54990584	0.64734876
KEGG_CYSTEINE_AND_METHIONINE_METABOLISM	0.2772554	0.91319263	0.5952849	0.6442672
KEGG_PROTEIN_EXPORT	0.3686309	0.89727354	0.59029126	0.65978324
KEGG_DRUG_METABOLISM_CYTOCHROME_P450	0.27977046	0.895435	0.61349696	0.65332603
KEGG_TERPENOID_BACKBONE_BIOSYNTHESIS	0.37947118	0.88096434	0.59100205	0.6673157
KEGG_LONG_TERM_POTENTIATION	0.265575	0.87706816	0.6404715	0.66389406
KEGG_ARGININE_AND_PROLINE_METABOLISM	0.25249606	0.8637797	0.6546906	0.67669934
KEGG_BASAL_TRANSCRIPTION_FACTORS	0.28742987	0.8605561	0.62081784	0.67225385
KEGG_CITRATE_CYCLE_TCA_CYCLE	0.33972847	0.8536729	0.60240966	0.67510945
KEGG_NOD_LIKE_RECEPTOR_SIGNALING_PATHWAY	0.27057242	0.8370338	0.6673077	0.6935009
KEGG_NITROGEN_METABOLISM	0.27890974	0.82567173	0.75390625	0.70317525
KEGG_DORSO_VENTRAL_AXIS_FORMATION	0.28094056	0.8064852	0.73410404	0.72584325
KEGG_TGF_BETA_SIGNALING_PATHWAY	0.24235316	0.7868584	0.71881187	0.7473405
KEGG_HUNTINGTONS_DISEASE	0.24811034	0.77978605	0.6855469	0.7484468
KEGG_PEROXISOME	0.23973116	0.75253385	0.7090559	0.7813006
KEGG_LINOLEIC_ACID_METABOLISM	0.24497381	0.6923127	0.8792757	0.8565561
KEGG_ANTIGEN_PROCESSING_AND_PRESENTATION	0.23718034	0.6906942	0.814	0.84799135
KEGG_OXIDATIVE_PHOSPHORYLATION	0.16179605	0.4302852	0.9700599	0.9947666

Supplementary Table 6B. GSEA of low risk.

NAME	ES	NES	NOM *p*-val	FDR *q*-val
KEGG_NEUROACTIVE_LIGAND_RECEPTOR_INTERACTION	−0.5290096	−1.890673	0	0.07818665
KEGG_TYPE_II_DIABETES_MELLITUS	−0.53263277	−1.7101595	0.003976143	0.41124317
KEGG_CALCIUM_SIGNALING_PATHWAY	−0.47805348	−1.7010419	0	0.3046739
KEGG_TRYPTOPHAN_METABOLISM	−0.5109064	−1.611668	0.0125	0.49959582
KEGG_GLYCINE_SERINE_AND_THREONINE_METABOLISM	−0.5354933	−1.5545669	0.045009784	0.6258049
KEGG_VASCULAR_SMOOTH_MUSCLE_CONTRACTION	−0.45131353	−1.5381501	0.033970278	0.5840838
KEGG_TASTE_TRANSDUCTION	−0.47686335	−1.5074612	0.050632913	0.61628556
KEGG_HEMATOPOIETIC_CELL_LINEAGE	−0.5428187	−1.4974189	0.08730159	0.57271385
KEGG_PRIMARY_IMMUNODEFICIENCY	−0.6386303	−1.4330411	0.18431373	0.75888455
KEGG_JAK_STAT_SIGNALING_PATHWAY	−0.43019027	−1.4310992	0.103658535	0.69109493
KEGG_ABC_TRANSPORTERS	−0.44498968	−1.4232751	0.06841046	0.65386295
KEGG_ADIPOCYTOKINE_SIGNALING_PATHWAY	−0.4124259	−1.4004673	0.07692308	0.6760876
KEGG_PHOSPHATIDYLINOSITOL_SIGNALING_SYSTEM	−0.43768927	−1.3972843	0.09850107	0.634523
KEGG_GLYCOSPHINGOLIPID_BIOSYNTHESIS_GANGLIO_SERIES	−0.54259735	−1.3912437	0.10261569	0.6088296
KEGG_INTESTINAL_IMMUNE_NETWORK_FOR_IGA_PRODUCTION	−0.5721416	−1.3898985	0.17773438	0.5723439
KEGG_MATURITY_ONSET_DIABETES_OF_THE_YOUNG	−0.55656147	−1.3844813	0.14003944	0.5516851
KEGG_CHEMOKINE_SIGNALING_PATHWAY	−0.4294434	−1.3836561	0.12704918	0.52157277
KEGG_ASTHMA	−0.5758721	−1.382636	0.17153996	0.49566385
KEGG_CELL_ADHESION_MOLECULES_CAMS	−0.43577835	−1.362344	0.17540322	0.5201028
KEGG_CYTOKINE_CYTOKINE_RECEPTOR_INTERACTION	−0.40754113	−1.3578213	0.12525667	0.5050087
KEGG_MTOR_SIGNALING_PATHWAY	−0.42019013	−1.3523698	0.106471814	0.49395788
KEGG_REGULATION_OF_AUTOPHAGY	−0.42233485	−1.3461435	0.10816327	0.48515308
KEGG_TYROSINE_METABOLISM	−0.42170665	−1.341936	0.10766046	0.47379693

KEGG_GLYCOSAMINOGLYCAN_DEGRADATION	−0.48054728	−1.3278168	0.15605749	0.48577037
KEGG_FC_EPSILON_RI_SIGNALING_PATHWAY	−0.39328453	−1.3148739	0.15212981	0.4949966
KEGG_PPAR_SIGNALING_PATHWAY	−0.38816133	−1.297917	0.1399177	0.51296306
KEGG_LONG_TERM_DEPRESSION	−0.36285532	-1.2761356	0.13279678	0.5412
KEGG_COMPLEMENT_AND_COAGULATION_CASCADES	−0.3989361	−1.263181	0.16384181	0.5521064
KEGG_TYPE_I_DIABETES_MELLITUS	−0.4928752	−1.2604029	0.26732674	0.53883076
KEGG_PROXIMAL_TUBULE_BICARBONATE_RECLAMATION	−0.44412115	−1.2592758	0.18590999	0.522951
KEGG_PRIMARY_BILE_ACID_BIOSYNTHESIS	−0.49527532	−1.2533015	0.18442623	0.51886904
KEGG_GNRH_SIGNALING_PATHWAY	−0.34357572	−1.2519171	0.14784394	0.50569147
KEGG_INOSITOL_PHOSPHATE_METABOLISM	−0.39771664	−1.2419469	0.21920668	0.51269734
KEGG_MAPK_SIGNALING_PATHWAY	−0.32389942	−1.2344974	0.1764706	0.51308984
KEGG_ALDOSTERONE_REGULATED_SODIUM_REABSORPTION	−0.3750422	−1.22868	0.16359918	0.5105368
KEGG_T_CELL_RECEPTOR_SIGNALING_PATHWAY	−0.411573	−1.2120905	0.28456914	0.5295486
KEGG_GLYCOSAMINOGLYCAN_BIOSYNTHESIS_CHONDROITIN_SULFATE	−0.45656192	−1.206142	0.2774451	0.52710754
KEGG_NICOTINATE_AND_NICOTINAMIDE_METABOLISM	−0.38467285	−1.2003758	0.23868313	0.52426314
KEGG_AUTOIMMUNE_THYROID_DISEASE	−0.43872103	−1.1698861	0.31547618	0.57136863
KEGG_MELANOGENESIS	−0.3255055	−1.1616304	0.23982869	0.57462007
KEGG_ALLOGRAFT_REJECTION	−0.5078549	−1.158935	0.36399218	0.56604004
KEGG_GAP_JUNCTION	−0.3317633	−1.1554563	0.26283368	0.55955046
KEGG_FATTY_ACID_METABOLISM	−0.40320912	−1.1531155	0.29012346	0.5516308
KEGG_SELENOAMINO_ACID_METABOLISM	−0.37339255	−1.1386981	0.30241936	0.56841093
KEGG_BETA_ALANINE_METABOLISM	−0.39741	−1.1361926	0.28252032	0.5608648
KEGG_GLYCEROPHOSPHOLIPID_METABOLISM	−0.31059223	−1.1272689	0.26612905	0.56516355
KEGG_OLFACTORY_TRANSDUCTION	−0.24886155	−1.115168	0.22376238	0.57648504
KEGG_PRION_DISEASES	−0.36823776	−1.1127352	0.3093385	0.56920344
KEGG_INSULIN_SIGNALING_PATHWAY	−0.3109605	−1.1121604	0.3268817	0.5585135
KEGG_BUTANOATE_METABOLISM	−0.37009233	−1.0814086	0.36491936	0.6072234
KEGG_PANTOTHENATE_AND_COA_BIOSYNTHESIS	−0.37421823	−1.0770823	0.3530572	0.6036107
KEGG_CARDIAC_MUSCLE_CONTRACTION	−0.32574925	−1.0768429	0.371134	0.5923154
KEGG_PROGESTERONE_MEDIATED_OOCYTE_MATURATION	−0.32766244	−1.0730956	0.36247334	0.588726
KEGG_VALINE_LEUCINE_AND_ISOLEUCINE_DEGRADATION	−0.37054572	−1.0679052	0.37623763	0.5874844
KEGG_DILATED_CARDIOMYOPATHY	−0.31053647	−1.0668976	0.34879032	0.5784172
KEGG_EPITHELIAL_CELL_SIGNALING_IN_HELICOBACTER_PYLORI_INFECTION	−0.31845626	−1.0656122	0.36916837	0.5703242
KEGG_GRAFT_VERSUS_HOST_DISEASE	−0.4773792	−1.0647981	0.42629483	0.56208354
KEGG_LYSINE_DEGRADATION	−0.3400369	−1.0595781	0.39591837	0.5619305
KEGG_FC_GAMMA_R_MEDIATED_PHAGOCYTOSIS	−0.32370082	−1.056988	0.3877551	0.55720764
KEGG_GLYCOSAMINOGLYCAN_BIOSYNTHESIS_HEPARAN_SULFATE	−0.36602896	−1.0548011	0.37708333	0.5525173
KEGG_ARACHIDONIC_ACID_METABOLISM	−0.30121955	−1.0340339	0.39314517	0.57759076
KEGG_RIBOFLAVIN_METABOLISM	−0.3628063	−1.0269295	0.41041666	0.58104
KEGG_B_CELL_RECEPTOR_SIGNALING_PATHWAY	−0.35677096	−1.0201818	0.45039684	0.5839937
KEGG_PHENYLALANINE_METABOLISM	−0.3458501	−1.0084561	0.44855967	0.59530926
KEGG_RENIN_ANGIOTENSIN_SYSTEM	−0.39185286	−0.9946408	0.48336595	0.61027443
KEGG_HISTIDINE_METABOLISM	−0.32132426	−0.9890151	0.48033127	0.6116145
KEGG_LYSOSOME	−0.30735183	−0.9859231	0.4526316	0.6080056
KEGG_VIBRIO_CHOLERAE_INFECTION	−0.2991553	−0.9856829	0.4556701	0.59937316
KEGG_PURINE_METABOLISM	−0.271922	−0.98382556	0.46637744	0.5934177
KEGG_RNA_POLYMERASE	−0.34659335	−0.95722973	0.50988144	0.6307953
KEGG_NEUROTROPHIN_SIGNALING_PATHWAY	−0.27906525	−0.92767113	0.56959313	0.67536575
KEGG_ACUTE_MYELOID_LEUKEMIA	−0.30859992	−0.92660505	0.54037267	0.66776955
KEGG_AMYOTROPHIC_LATERAL_SCLEROSIS_ALS	−0.27340278	−0.92612875	0.5708419	0.6596064
KEGG_NON_SMALL_CELL_LUNG_CANCER	−0.30022708	−0.92514	0.55737704	0.65228117
KEGG_LEUKOCYTE_TRANSENDOTHELIAL_MIGRATION	−0.27998474	−0.9202179	0.5386266	0.6523266
KEGG_ERBB_SIGNALING_PATHWAY	−0.26887137	−0.91797024	0.5744235	0.6477343
KEGG_HEDGEHOG_SIGNALING_PATHWAY	−0.28201923	−0.9156276	0.55737704	0.64300805
KEGG_NATURAL_KILLER_CELL_MEDIATED_CYTOTOXICITY	−0.28414455	−0.90748185	0.54969573	0.6490106
KEGG_SPHINGOLIPID_METABOLISM	−0.29363042	−0.9023531	0.60162604	0.6489709

KEGG_PROPANOATE_METABOLISM	−0.3202926	−0.8933692	0.59356135	0.6564102
KEGG_GLIOMA	−0.26588964	−0.87776834	0.6012397	0.67394316
KEGG_GLYCEROLIPID_METABOLISM	−0.25562853	−0.87741315	0.645749	0.66659164
KEGG_OTHER_GLYCAN_DEGRADATION	−0.3497702	−0.8746694	0.5978947	0.6635369
KEGG_LEISHMANIA_INFECTION	−0.31960237	−0.8571332	0.6122449	0.6853992
KEGG_ALANINE_ASPARTATE_AND_GLUTAMATE_METABOLISM	−0.26438203	−0.8277334	0.71398747	0.72542256
KEGG_VIRAL_MYOCARDITIS	−0.27853227	−0.82128996	0.62890625	0.7271384
KEGG_TOLL_LIKE_RECEPTOR_SIGNALING_PATHWAY	−0.25039133	−0.80701625	0.66935486	0.7418337
KEGG_RIG_I_LIKE_RECEPTOR_SIGNALING_PATHWAY	−0.24272378	−0.7962348	0.71666664	0.7515454
KEGG_VASOPRESSIN_REGULATED_WATER_REABSORPTION	−0.257244	−0.7952852	0.7171717	0.7445486
KEGG_SNARE_INTERACTIONS_IN_VESICULAR_TRANSPORT	−0.26335508	−0.79454243	0.71369296	0.7376034
KEGG_PYRUVATE_METABOLISM	−0.25223786	−0.79080826	0.73140496	0.7351275
KEGG_GLYCOSYLPHOSPHATIDYLINOSITOL_GPI_ANCHOR_BIOSYNTHESIS	−0.29210636	−0.7644893	0.72938687	0.76874876
KEGG_ALPHA_LINOLENIC_ACID_METABOLISM	−0.2534912	−0.7415896	0.87829614	0.79504913
KEGG_GLYOXYLATE_AND_DICARBOXYLATE_METABOLISM	−0.29077378	−0.7335219	0.78644764	0.79881746
KEGG_CYTOSOLIC_DNA_SENSING_PATHWAY	−0.23144941	−0.7221297	0.8114754	0.80624986
KEGG_RIBOSOME	−0.3269558	−0.6639908	0.7683168	0.8751104
KEGG_PARKINSONS_DISEASE	−0.18312952	−0.5185772	0.92785573	0.9770979